Transactions of Tianjin University (2024) 30:518–543
https://doi.org/10.1007/s12209-024-00419-9

REVIEW

Functionalization Strategies of Iron Sulfides for High-Performance Supercapacitors

Can Wang[1] · Yuxin Zhang[1] · Shude Liu[2] · Danping Wang[3]

Received: 15 May 2024 / Revised: 11 June 2024 / Accepted: 27 June 2024 / Published online: 7 November 2024

Abstract

Supercapacitors have emerged as a promising class of energy storage technologies, renowned for their impressive specific capacities and reliable cycling performance. These attributes are increasingly significant amid the growing environmental challenges stemming from rapid global economic growth and increased fossil fuel consumption. The electrochemical performance of supercapacitors largely depends on the properties of the electrode materials used. Among these, iron-based sulfide (IBS) materials have attracted significant attention for use as anode materials owing to their high specific capacity, eco-friendliness, and cost-effectiveness. Despite these advantages, IBS electrode materials often face challenges such as poor electrical conductivity, compromised chemical stability, and large volume changes during charge–discharge cycles. This review article comprehensively examines recent research efforts aiming at improving the performance of IBS materials, focusing on three main approaches: nanostructure design (including 0D nanoparticles, 1D nanowires, 2D nanosheets, and 3D structures), composite development (including carbonaceous materials, metal compounds, and polymers), and material defect engineering (through doping and vacancy introduction). The article sheds light on novel concepts and methodologies designed to address the inherent limitations of IBS electrode materials in supercapacitors. These conceptual frameworks and strategic interventions are expected to be applied to other nanomaterials, driving advancements in electrochemical energy conversion.

Keywords Anode materials · Supercapacitors · Electrochemical performance · Nanostructures · Carbonaceous materials

Introduction

In the wake of increasing fossil fuel depletion and ensuing environmental crises, the pivot toward renewable and clean energy sources has garnered global attention, emerging as pivotal subjects of scholarly inquiry [1–8]. Solar, wind, and tidal energies, alongside hydrogen fuel, hold promise to mitigate the adverse effects stemming from fossil fuel consumption, such as dwindling reserves, rising global temperatures, and exacerbating environmental degradation [9–13]. However, these clean energy sources face challenges regarding their stability [14–17], underscoring the need for advanced electrochemical energy storage solutions that boast high-energy density, efficiency, flexibility, and operational flexibility. Electrochemical double-layer capacitors (EDLCs), colloquially referred to as supercapacitors, have garnered the interest of the research community owing to their broad spectrum of applications in energy consumption, generation, and storage. As depicted in Fig. 1a, illustrating the Ragone graph delineating energy density in Wh/kg vs power density in W/kg, supercapacitors (SCs) exhibit distinct advantages compared to conventional batteries. In particular, they are capable of attaining theoretical capacities in the order of several thousand farads via constrained cell voltage [18–24]. Despite their relatively low cell voltage and energy density, supercapacitors excel in providing high power density, thermal stability, low impedance, and

✉ Yuxin Zhang
zhangyuxin@cqu.edu.cn

✉ Shude Liu
sdliu@dhu.edu.cn

[1] College of Materials Science and Engineering, Chongqing University, Chongqing 400044, China

[2] Engineering Research Center of Technical Textiles, Ministry of Education, Shanghai Frontiers Science Center of Advanced Textiles, College of Textiles, Donghua University, Shanghai 201620, China

[3] Singapore Institute of Technology, Singapore 138683, Singapore

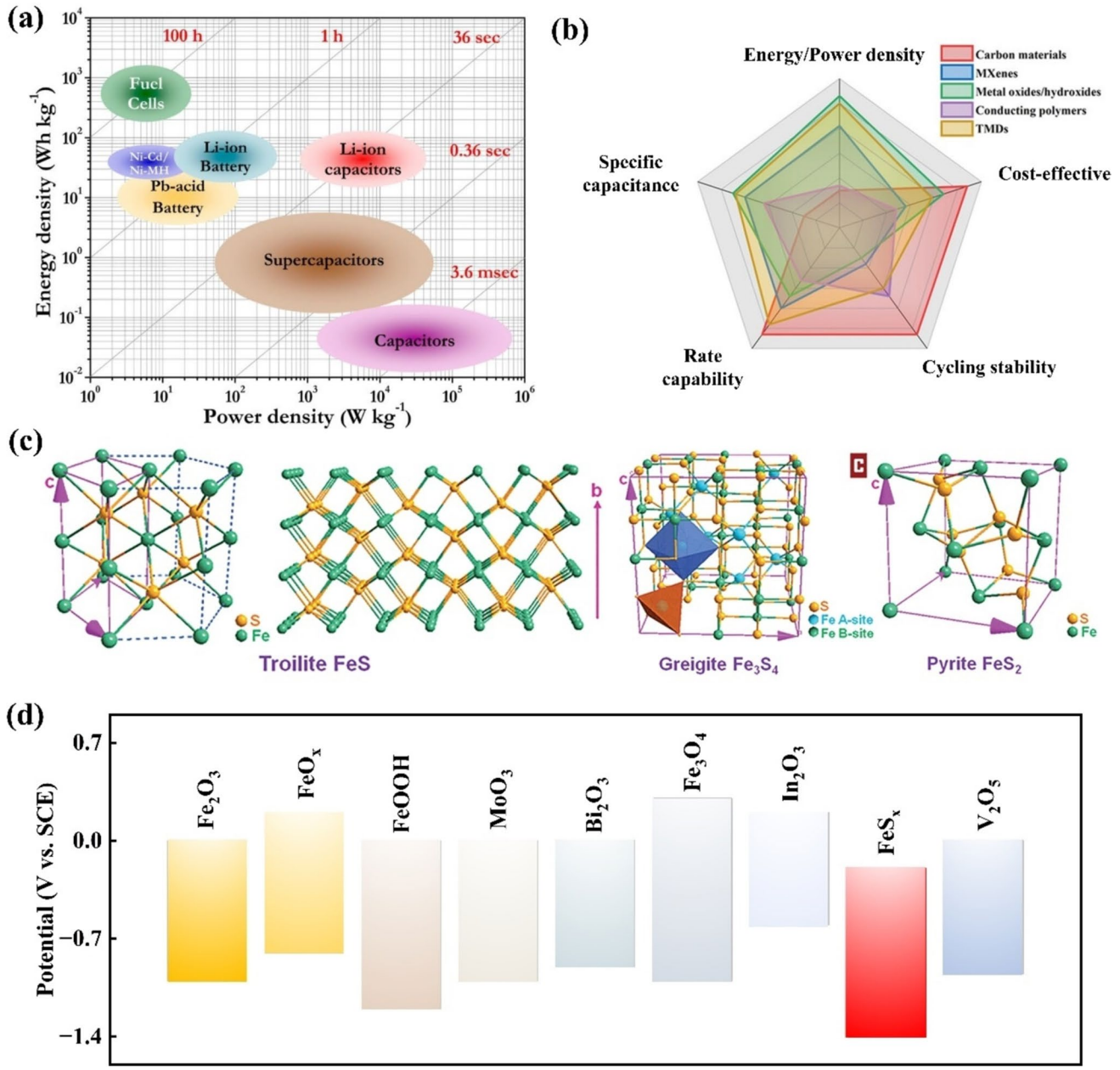

Fig. 1 **a** Ragone plot depicting the performance characteristics of specific power versus specific energy for various electrical energy storage technologies. Times indicated on the plot represent discharge times, calculated by dividing the energy density by the power density; **b** radar chart illustrating carbon material properties, MXenes, metal oxides/hydroxides, conducting polymers, and transition metal dichalcogenides (TMDs). The properties range from poor to good, progressing from the inner to the outer regions Reproduced with permission from Ref. [31]. [33–39] Copyright © 2024, Wiley; **c** Crystal structures of stoichiometric iron sulfides (from left to right: troilite FeS along different directions, greigite Fe_3S_4, and pyrite FeS_2) Reproduced with permission from Ref. [32]. Copyright © 2014, Royal Society of Chemistry; **d** potential windows of operation for various electrode materials in an aqueous electrolyte

remarkable cycle life. These attributes render them invaluable across diverse industrial domains, encompassing electric vehicles and solar energy plants [25–30].

Carbon materials, commonly encompassing activated carbon (AC) [40, 41], carbon nanotubes [42, 43], and graphene [44, 45], serve as the backbone for EDLCs, where charge is stored through iron adsorption at the electrode–electrolyte interface, exemplifying a typical mechanism [46]. Conversely, pseudocapacitors (PCs) rely on rapid and reversible redox reactions for charge storage, employing materials such as conducting polymers [47, 48], transition metal oxides and hydroxides [49, 50], MXenes [51, 52], and transition metal sulfides [53–55]. TMDs, as illustrated in Fig. 1b, have been recognized for their exceptional performance as

supercapacitor electrode materials, outshining conventional capacitive materials. Additionally, metal sulfides, particularly iron-based sulfides (IBSs), have emerged as prominent candidates for SCs owing to their complex redox chemistry that enables higher specific capacities or capacitances compared to other TMDs [56–59]. Moreover, they boast superior electrical conductivity, mechanical strength, and thermal stability when compared to their metal oxide counterparts, marking a significant advancement in electrode material selection. IBSs have garnered significant interest as potential electrode materials for supercapacitors owing to their advantageous characteristics. Their appeal lies in the multiple valence states of iron (Fe^0, Fe^{2+}, Fe^{3+}), which facilitate a rich redox chemistry, including transitions such as Fe^0/Fe^{2+}, Fe^0/Fe^{3+}, and Fe^{2+}/Fe^{3+}. This extensive redox activity enables IBSs to achieve high specific capacitance [60–64]. The rising interest in IBSs is evidenced by the increased number of research publications and citations over the past decade. The Fe–S phase diagrams depicted in Fig. 1c elucidate the diverse stoichiometries and crystal structures of the four iron sulfides, which vary with temperature, pressure, and sulfur concentration [32]. Compounds like FeS, Fe_3S_4, and FeS_2 have been extensively studied as potential high-capacity anode materials for supercapacitors [65–67]. Furthermore, IBSs have been extensively investigated for their high electrochemical properties, low toxicity, and elevated specific capacity [31]. According to previous reports, the Faradaic redox processes can be attributed to the FeS/FeSOH and FeSOH/FeSO transitions. The corresponding equations are shown below [15, 18, 30]:

$$FeS_x + OH^- \rightleftharpoons FeS_xOH + e^- \quad (1)$$

$$FeS_xOH + OH^- \rightleftharpoons FeS_xO + H_2O + e^- \quad (2)$$

Recent advancements in electrode materials for supercapacitors, particularly those based on transition metal oxides, hydroxides, and sulfides, have been notable. This progress is captured in the analysis of the typical operating potential windows of these materials, as illustrated in Fig. 1d [60, 68–74]. Notably, IBSs warrant further investigation compared to other iron-based materials. Simultaneously, they offer a stable and broad operating window at negative potentials, rendering them highly promising candidates for high-performance negative electrodes in supercapacitors [75–79].

This study aims to provide a comprehensive review of the methodologies employed to enhance the suboptimal performance of IBS materials and their properties. Special emphasis is placed on the latest synthetic approaches developed over the past five years, designed to address the specific challenges confronting IBSs, as delineated in Fig. 2. Despite the proliferation of high-quality reviews on the synthesis and application of IBSs in supercapacitors, there has been a noticeable gap in the literature regarding detailed discussions on remedial approaches for the issues associated with IBSs. While certain reviews have touched upon the preparation and potential applications of iron sulfides, they have predominantly emphasized the advanced properties and preparation techniques of IBSs, leaving a void in the systematic evaluation of solutions aimed at improving the electrochemical performance of IBS nanocomposites. The core objective of this review article is to shine a light on the efforts to enhance the electrochemical performance of IBS nanomaterials for use as electrodes in supercapacitors. Through various methodologies, remarkable electrochemical performances have been attained, and our objective is to delineate these achievements.

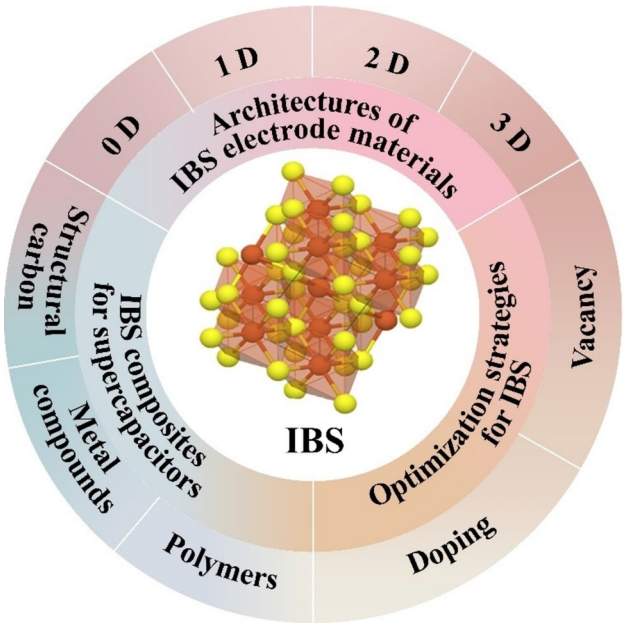

Fig. 2 Schematic representation outlining diverse enhancements utilized for IBSs to attain exemplary electrochemical energy storage performance

Architectures of IBS Electrode Materials

In this section, we delve into various strategies for fabricating IBS materials into nanostructures spanning different dimensions. We emphasize how these diverse nanostructures enhance the electrochemical properties of the materials. A rational research and development endeavor is directed toward devising and customizing novel IBSs possessing 0D, 1D, 2D, and 3D morphologies. Such morphological diversity is engineered to optimize surface areas, shorten diffusion pathways, and increase the availability of ion-interacting active sites. These modifications are vital for achieving optimal specific capacitance. The fabrication of

IBS materials into 0D, 1D, and 2D morphologies is geared toward enhancing their suitability for intercalation and de-intercalation phenomena. This is attributed to their ability to offer restricted diffusion, flexibility, and extensive surface availability. Conversely, 3D materials distinguish themselves by offering a plethora of reaction sites, thereby contributing to enhanced energy and power density. The prevalent techniques for fabricating these 0–3D nanostructured IBSs have been succinctly outlined and categorized, as depicted in Fig. 3.

0D Nanostructures

Zero-dimensional (0D) structured materials are advantageous for use as electrodes in supercapacitors owing to their notable properties. These materials exhibit relatively short electron transport paths owing to their sizes, which in turn reduces resistance and enhances the charge transfer rate. Additionally, 0D structured materials typically possess a very high specific surface area, which significantly enhances the amount of active material to be in contact with the electrolyte for a given volume or mass. This trait increases the interfacial area between the electrode and the electrolyte, thereby improving the charge storage capacity. [47, 63, 67] Nanoparticles, quantum dots, and nano-clusters are three types of 0D morphologies to iron-sulfide materials in usual, with extremely high activity.

Recently, Wang et al. [80] immobilized FeS_2/CoS_2 nanoparticles on porous carbon derived from kelp through heating Fe^{3+} and Co^{2+} ions. The porous carbon showcases an average particle size distribution ranging between 500 and 900 nm, as shown in Fig. 4a and b. Its hierarchical honeycomb structure within the kelp-derived porous carbon acts as a reservoir for electrolyte ions, effectively shortening the diffusion pathway of these ions, facilitating charge transfer, and ensuring the FeS_2/CoS_2 nanoparticles remain immobilized during electrochemical reactions. This integration of metal disulfides with conductive porous carbon mitigates volume expansion during charge–discharge cycles and improves the overall electrochemical performance. Moreover, the addition of graphene has been shown to significantly improve IBS performance. Turali-Emre et al. [81] successfully

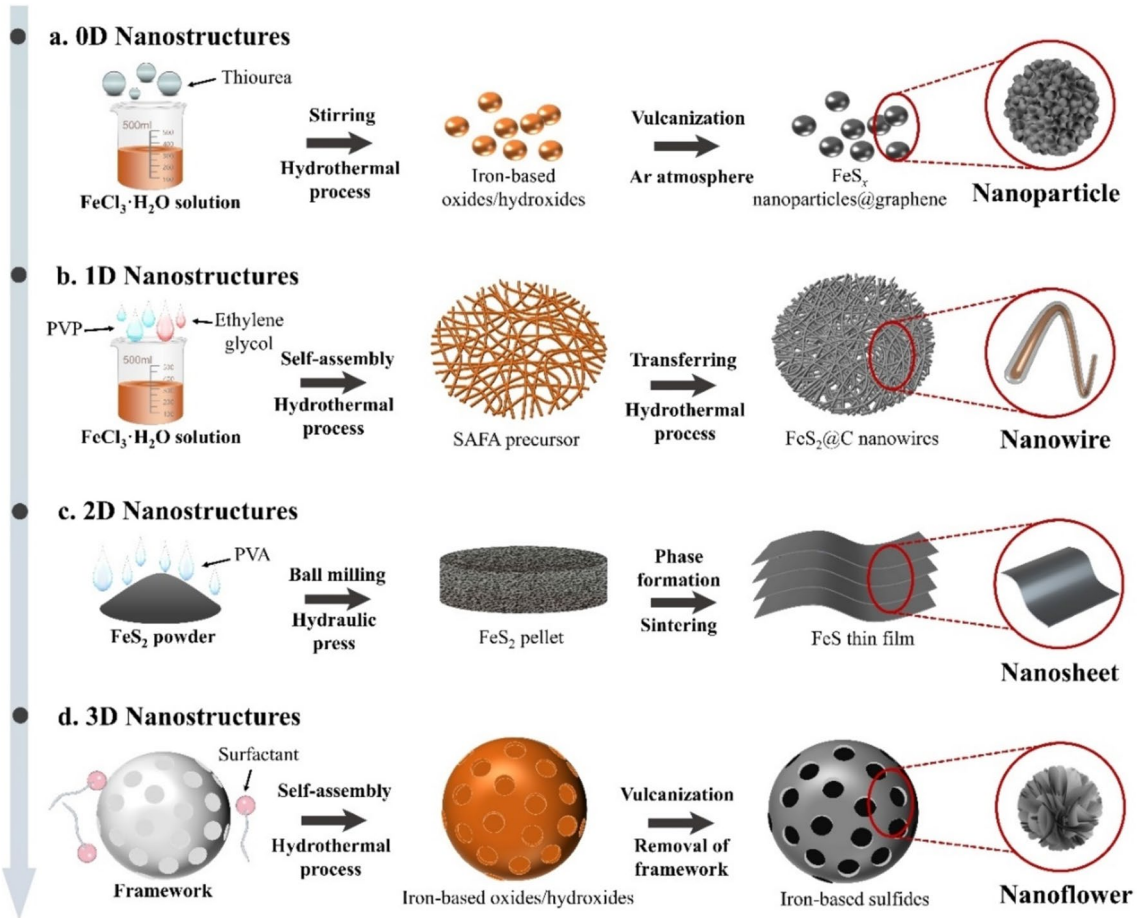

Fig. 3 Common preparation methods for 0D–3D architectures of IBS electrode materials: **a** 0D nanoparticles, **b** 1D nanowires, **c** 2D nanosheets, and **d** 3D nanoflowers

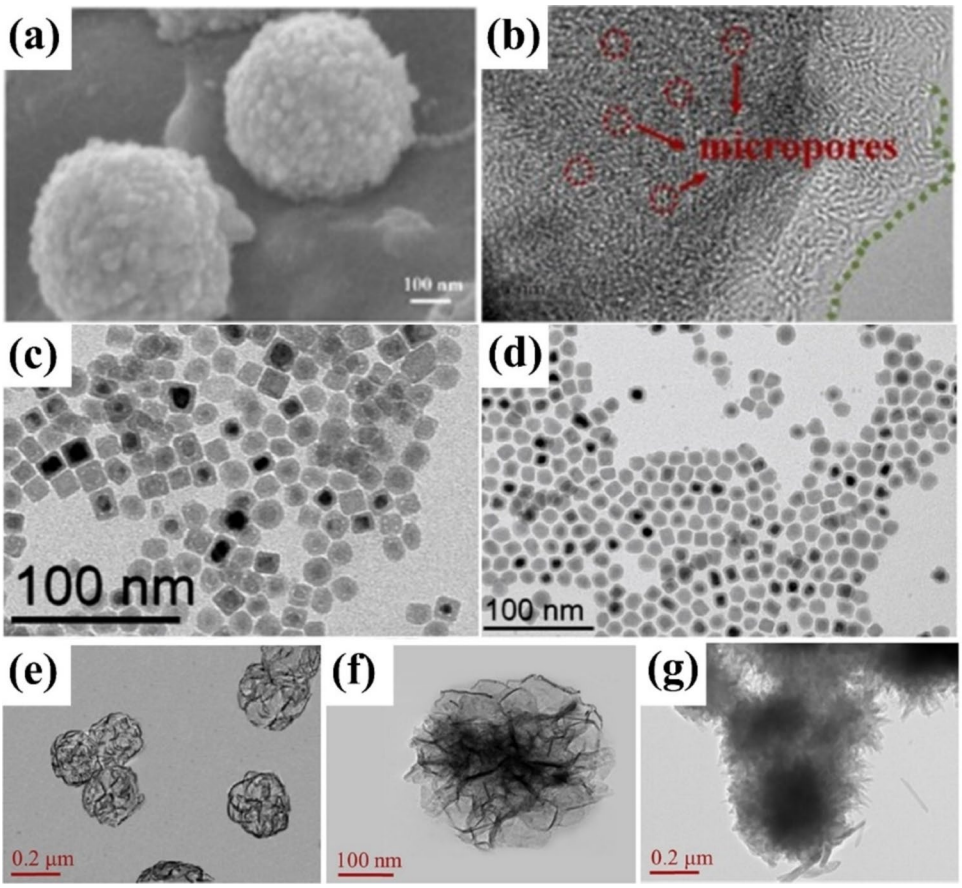

Fig. 4 **a** SEM image, and **b** TEM image of FeS_2/CoS_2@KC-800 Reproduced with permission from Ref. [80] Copyright © 2023, Elsevier; TEM pictures of core–shell particles **c** 5A and **d** 5B obtained in sulfidation reactions of 13 nm zerovalent iron NPs with benzyl thiol after 18 h and 4 h, respectively Reproduced with permission from Ref. [82] Copyright © 2018, Wiley–VCH; TEM images of **e** NSA–FeS_2, **f** high-resolution lattice image of NSA–FeS_2 and **g** NSA–FeS_2/PANI Reproduced with permission from Ref. [84] Copyright © 2023, American Chemistry society

synthesized FeS_2 nanoparticles through a process that inhibited their spontaneous self-assembly. The newly prepared iron-sulfide nanoparticles display an electrokinetic zeta potential of $\zeta = +20.5 \pm 1.5$ mV and have a disk-like geometry with a diameter of 4.5 ± 1.6 nm and a height of approximately 1.5 nm, as determined via transmission electron microscopy. Chaudret et al. [82] prepared iron-sulfide nanocomposites through reactions of bis[bis(trimethylsilyl) amido]iron(II) or zerovalent iron nanoparticles with hydrogen sulfide. TEM pictures of core–shell particles 5A and 5B were obtained in sulfidation reactions of 13 nm zerovalent iron nanoparticles with benzyl thiol after 18 h and 4 h, as shown in Fig. 4c and d, respectively. Tuček et al. [83] used a rapid growth method on highly functionalized graphene support to firmly anchor ultrasmall greigite (Fe_3S_4) nanoparticles, which could not be achieved without the use of graphene. GCNFe_3S_4 has a typical gray mica mixed-valence spinel structure characterized by the basic structural unit of thiocarban. This novel 0D electrode exhibits outstanding performance in rate capacity and cycling stability. Jung et al. [84] fabricated nanosheet-assembled FeS_2 (NSA–FeS_2) through a novel method. They generated sub-micron droplets of sulfur particles stabilized with polyvinylpyrrolidone in a silicone oil medium. $Fe(CO)_5$ was then absorbed and reacted on the surface of these droplets to form core–shell particles, ES/[Fe], with a sulfur core and an iron-containing outer shell. High-temperature treatment of ES/[Fe] produced NSA–FeS_2 (Fig. 4e and f), in which pyrite FeS_2 nanosheets grew and were partially interconnected. Tested in a three-electrode system, the newly prepared NSA–FeS_2 and NSA–FeS_2/polyaniline (PANI) composites (Fig. 4g) exhibited specific capacitances of 763 and 976 F/g, respectively, at a current density of 0.5 A/g, maintaining capacitance retentions of 93% and 96% after 3000 charge–discharge cycles. Additionally, Cai et al. [85] explored a simple and fat solid-phase reaction to create FeS/C composites, using starch as both a dispersant and carbon source. The resultant composite showcased an exceptional specific capacitance of 275.65 F/g and maintained up to 90% of its maximum specific capacitance after 1000 electrochemical cycles. These studies underscore how 0D structured materials can effectively form active sites and pair with multi-dimensional substrate materials, such as porous carbon and graphene, to achieve excellent ionic conductivity. This significantly enhances supercapacitor performance.

1D Nanostructures

1D structured materials stand out for their exceptional electron transport properties, which directly contribute to the

rapid charging and discharging capabilities of supercapacitors, as well as an increase in power density. Their advantageous mechanical properties make them versatile in electrode design, adapting to various shapes and sizes, thereby enhancing electrode reliability and durability. The large aspect ratio and high specific surface area of 1D structured materials endow them with a higher number of active sites for charge storage, thereby increasing the energy density of supercapacitors [42–44, 71, 72]. 1D morphologies are often nanowires, nanotubes, and nanofibers, which are typically fabricated using hydrothermal in situ synthesis.

For example, Wang et al. [86] successfully synthesized 1D FeS_2@C nanowires from organo-inorganic hybrid SAFA nanowires, as shown in Fig. 5a and b. Thanks to the synergistic advantages of the 1D porous nanostructures combined with a thin amorphous carbon layer, these FeS_2@C nanowires shortened the diffusion path of lithium ions. The amorphous carbon layer can effectively prevent polysulfide dissolution during the cycling process and increase conductivity, thereby overcoming typical challenges confronting the FeS_2 cathode. Consequently, FeS_2@C nanowires demonstrate high reversible capacity, excellent rate capability, and stable cycling performance. The SEM images of FeS_2@C electrode at full discharge after 10 cycles at 0.1 A/g and at full charge state after 10 cycles at 0.1 A/g demonstrated that FeS_2@C nanowires retain their original nanowire morphology before and after cycling. In addition, introducing composite carbon nanofibers has been shown to effectively improve the small specific capacity of IBSs. Huang et al. [87] have rationally synthesized lawn-like $FeCo_2S_4$ hollow nanopin arrays (HNNA) on flexible carbon nanofiber (CNF) films via a two-step hydrothermal method. These unique hollow structures and stable tip-welded $FeCo_2S_4$ nanopins, uniformly deposited on conductive CNF films as shown in Fig. 5c and d, provide a large number of electroactive sites and short pathways for electrolyte transport, enhancing energy storage efficiency and accommodating shape changes during charge and discharge cycles. The porous CNF films facilitate homogeneous nucleation of $FeCo_2S_4$ nanopins, ensuring fast charge transfer pathways for electrochemical processes and acting as powerful current collectors for binder-free electrodes. Such features enable the $FeCo_2S_4$ HNNA/CNF composite electrode to exhibit a high specific capacitance of 2476 F/g at 1 A/g. The supercapacitor device based on this composite film also offers a high-energy density of 88.5 Wh/kg at 800 W/kg and excellent cycling stability with capacitance retention of 81.2% after 5000 charge/discharge cycles. Wang et al. [88] prepared FeS–CNF composites through electrostatic spinning and hydrothermal methods, highlighting its high specific capacitance (502 F/g at a current density of 2 A/g), good cycling stability (90% capacitance retention after 1000 cycles), and excellent multiplicative properties, with capacitance retention up to 401 F/g at a current density of 10 A/g. The SEM images of carbonized Fe–CNF fibers before and after FeS–CNFs are shown in Fig. 5e and f, respectively. These improvements are largely attributed to the carbon fibers' increased specific surface area and provision of a higher number of electrochemically

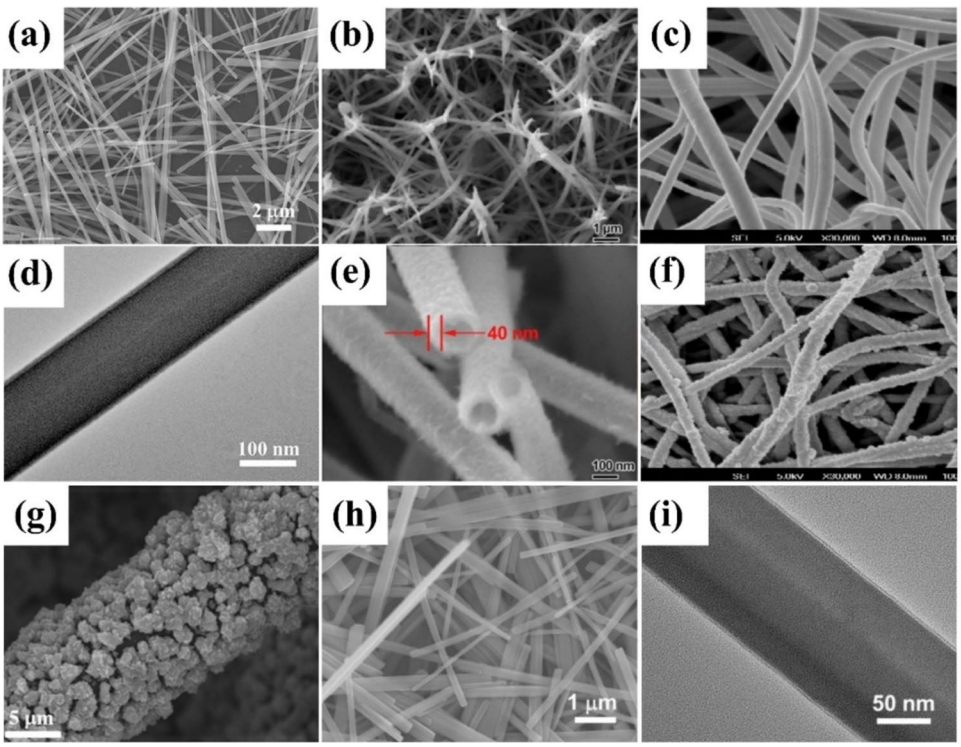

Fig. 5 **a** SEM images and **b** TEM images of the precursor SAFA nanowires; **c** SEM images of a $FeCo_2S_4$ HNNA/CNF composite film: deposited lawn-like $FeCo_2S_4$ hollow nanoneedle arrays; **d** SEM of ultrasonically broken $FeCo_2S_4$ hollow nanoneedles Reproduced with permission from Ref. [87] Copyright © 2019, Elsevier; **e** SEM images of carbonized Fe–CNF fibers; **f** FeS–CNFs Reproduced with permission from Ref. [88] Copyright © 2020, Springer Heidelberg; **g** SEM images of P/Co–FeS_2 nanocomposites on CFP Reproduced with permission from Ref. [89] Copyright © 2017, Wiley; **h** Scanning electron microscopy (SEM) and **i** TEM images of the FeS_2–ethylenediamine precursor Reproduced with permission from Ref. [90] Copyright © 2019, MDPI

active centers for ion intercalation or delamination, thus improving the electrochemical properties of the material. Kuo et al. [89] introduced a Co–FeS_2 catalyst with surface phosphide doping (P/Co–FeS_2), showing nanocomposite particle morphology with an average size of approximately 100 nm (Fig. 5g). Furthermore, Pan et al. [90] synthesized the FeS_2/C catalyst featuring a porous nanostructure through a meticulously designed in situ electrochemical activation method. This approach yielded FeS_2–amine nanowires with diameters d of approximately 100 nm and lengths stretching up to tens of micrometers, characterized by a highly uniform nanowire morphology and a fairly smooth surface (Fig. 5h). Polyvinylpyrrolidone (PVP), a substance commonly used for chemical reduction or to steer the 3D structure formation of products, played a crucial role in this synthesis. The lone electron pairs of oxygen present in PVP can donate and coordinate with Fe ions during the reaction process. The FeS_2–ethylenediamine precursor showcased through TEM imaging a 5-nm amorphous and uniform outer layer (Fig. 5i). 1D nanostructures can reduce the distance for ion/electron transport, which is vital for improving reaction kinetics and active substance utilization. Additionally, the increased specific surface area provides abundant electrochemical active sites [91]. Therefore, excellent electrochemical performance can be obtained by constructing reasonable 1D nanostructures.

2D Nanostructures

Two-dimensional (2D) structured materials offer numerous advantages for supercapacitor electrodes, including high specific surface area, excellent electrical conductivity, superior electrochemical stability, and significant customizability. The ability to tailor these materials through methods like doping, compounding, or modulating their layer spacing adds a layer of flexibility that can optimize electrode performance. By adjusting the layer spacing of 2D materials, one can effectively enhance ion diffusion and storage capabilities within the electrodes, thereby improving the overall efficiency and capacity of supercapacitors [33, 38, 59, 61]. These properties are further improved when they are structured into 2D nanoforms, which possess large specific surface areas and numerous active sites.

Within this category, materials such as nano-films, which can move freely within the 2D nanoscale range of 1–100 nm, have shown particular promise. Vadivel et al. [92] created a CNT/$FeNiS_2$@PPy nanotube@nanodisk heterostructure, showcasing a simple and cost-effective hydrothermal and polymerization method for creating what is described as an efficient electrode option for Ni foam. The $FeNiS_2$ morphology is shown in Fig. 6a. Ma et al. [93] utilized graphene oxide and thioglycolic acid (TGA) to prepare a 3DSG composite material with a distinct pore structure, a large specific surface, and specific capacitive properties using a one-step microwave method. To synthesize more efficient battery-type capacitor electrode materials, $NiFeS_2$/3DSG composites were simultaneously synthesized by adding Ni and Fe precursors during the microwave process. The small size and uniform dispersion of $NiFeS_2$ nanoparticles on the 3DSG surface, coupled with the use of TGA as a sulfur source for both 3DSG and $NiFeS_2$, made the synthesis process more efficient. The resulting $NiFeS_2$/3DSG composites exhibited high specific capacitance, excellent multiplicative capability, and long cycle stability, especially for hybrid asymmetric supercapacitor devices with competitive energy and power densities.

2D thin metal sulfide nanostructures have emerged as powerful materials for enhancing electrochemical reversible reactions and possessing a high theoretical capacity, making them highly suitable for flexible energy storage devices. Velmurugan et al. [94] demonstrated the excellent energy storage capabilities and electrocatalytic oxygen evolution reaction potential of an in situ troilite 2H phase FeS thin film nanostructure with a thickness of 250 nm, utilizing the pulsed laser deposition (PLD) technique. The process involves a PLD coating technique for depositing FeS thin films, providing detailed insight into the deposition mechanism and showcasing the morphological image of the troilite 2H phase FeS (A650) thin film, as shown in Fig. 6b–e. Further analysis using TEM and HRTEM offered a deeper understanding of the nanostructural aspects of FeS RT (Fig. 6b and c) and FeS (A650) (Fig. 6d and e) thin films, each coated on carbon paper substrates. Yan et al. [95] prepared ultrathin single-crystalline Fe-doped nickel thiophosphate ($NiPS_3$) nanosheets using a simple solid-state method, achieving large-scale production, as shown in Fig. 6f and g. The resultant nanosheets demonstrated good electrochemistry performance. Lu et al. [96] reported a novel FeS–NiS hybrid nanosheet array embedded on a Ti mesh. This hybrid serves as a highly efficient non-noble-metal electrocatalyst, which can improve supercapacitor performance, as shown in Fig. 6h and i. Therefore, 2D nanostructures can effectively increase the specific surface area and electrochemical activity center of the material. Furthermore, while compounded with 2D matrix materials, they significantly improve the electrochemical performance of the material.

3D Nanostructures

3D structured materials offer a higher specific surface area, significantly increasing the contact area between the electrode and the electrolyte. This increase in contact area provides a higher number of active sites available for charge storage and, coupled with the typical porosity of 3D structures, significantly facilitates the rapid transport and penetration of electrolyte ions, thereby reducing internal resistance.

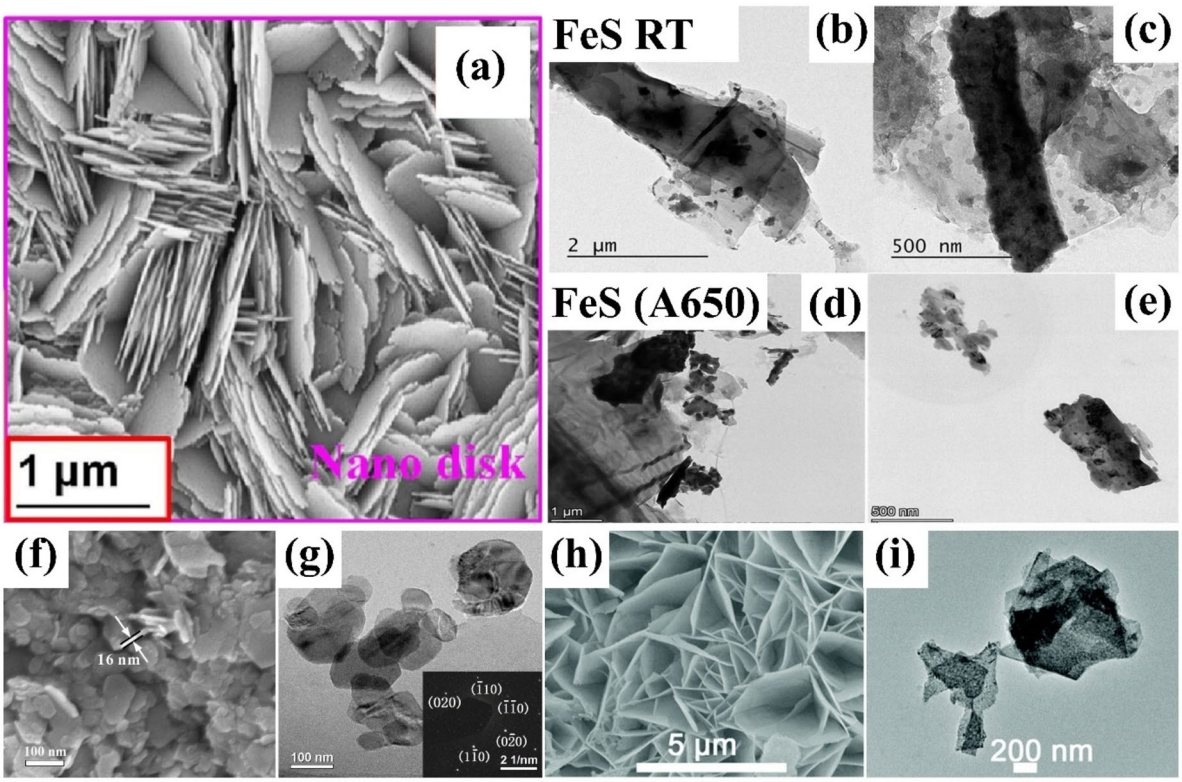

Fig. 6 **a** FESEM image of the $FeNiS_2$ material Reproduced with permission from Ref. [92] Copyright © 2023, Elsevier; **b, c** HRTEM analysis: TEM morphologies of the FeS RT thin film; **d, e** TEM morphologies for FeS (A650) thin film Reproduced with permission from Ref. [94] Copyright © 2023, Royal Society of Chemistry; **f** High-magnified SEM; **g** TEM images of the Fe-doped $NiPS_3$ nanosheets Reproduced with permission from Ref. [95] Copyright © 2018, Elsevier; **h** SEM images of FeS–NiS/TM and **i** TEM image of a FeS–NiS nanosheet Reproduced with permission from Ref. [96] Copyright © 2019, Royal Society of Chemistry

Furthermore, advanced fabrication techniques, such as template methods, offer precise structural control over the design and structure of 3D materials, enhancing their performance and suitability for supercapacitors [25, 50]. The 3D morphology of iron-based sulfide materials plays a crucial role in enhancing their electrochemical performance for energy storage applications.

Zhang et al. [97] proposed a simple and controllable method for synthesizing $KFeS_2$ with a diatomite morphology using a multistep sacrificial template. Diatomite, chosen for its high porosity, low volumetric weight, chemical stability, and high specific surface area (SSA), served as an excellent sacrificial template [98, 99]. Additionally, the 3D structure of diatomite effectively prevents material agglomeration [100–102]. The morphology of the products is shown in Fig. 7a and b. As shown in Fig. 7b, the end product retained a diatomite-like round cake shape that consisted of numerous interconnected nanosheets, forming a porous structure that significantly enhanced the SSA of $KFeS_2$, crucial for improving its electrochemical properties. Ye et al. [103] synthesized a GA-supported flower-like FeS_2 composite (GA–FeS_2) via a two-step self-assembly process, starting with the preparation of graphene oxide (GO) following the modified Hummers method as in previous reports [104]. Exfoliation of GO in deionized (DI) water was carried out through ultrasonication. The GA-FeS_2 composite was synthesized through a two-step self-assembly method. SEM images, as depicted in Fig. 7c and d, showcase the micro-morphology of the newly prepared GA-FeS_2. Within this structure, flower-like FeS_2 clusters, measuring 1–2 μm, are uniformly spread across the interconnected RGO sheets, exhibiting no obvious agglomeration. The fabrication process involves Fe^{2+} ions adhering to the GO sheets, compelling them to organize into a specific order. This self-assembled structure, retained by the subsequent reduction phase, effectively prevents the RGO sheets from aggregation, resulting in a cohesive GA morphology [105]. Figure 7d offers a closer look at the structure of a flower-like FeS_2 cluster, revealing its composition of numerous nanorods and nanoplates, each about 100 nm in size. For practical application evaluation, GA-FeS_2 was utilized as the electrode material in constructing a simple symmetric supercapacitor device. This supercapacitor containing GA-FeS_2 exhibited excellent performance, benefiting from the

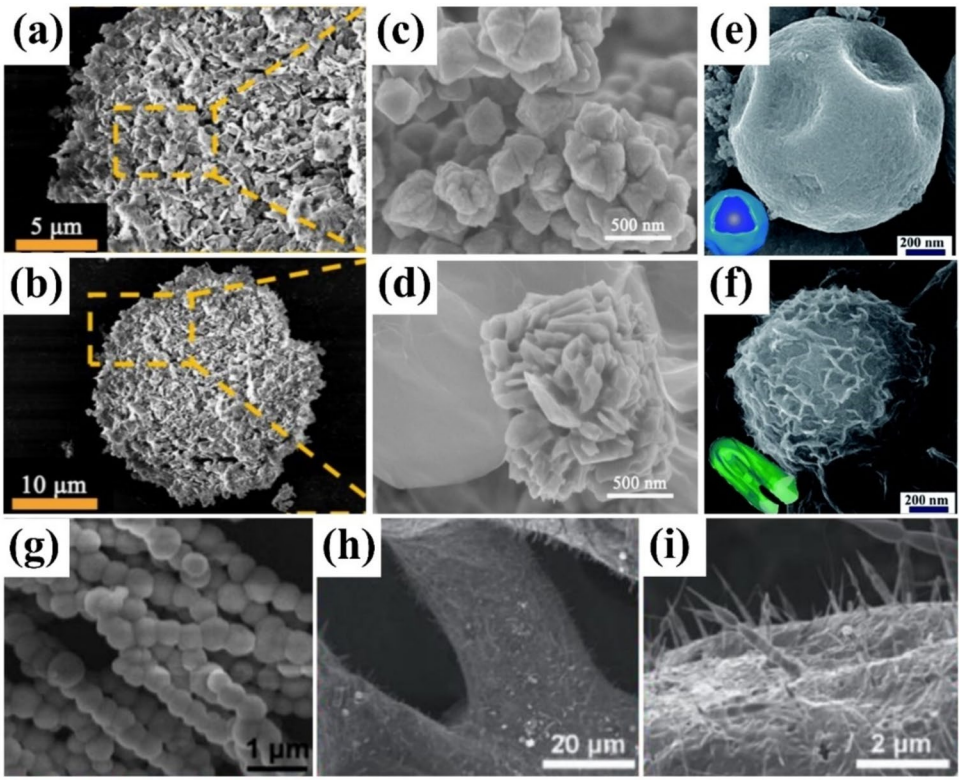

Fig. 7 **a**, **b** Magnification increases for the SEM images of the diatomite-like $KFeS_2$ Reproduced with permission from Ref. [97] Copyright © 2023, MDPI; **c**, **d** SEM images of the newly prepared GA–FeS_2 in low and high magnification; **e** high-magnification FE–SEM image of the FeS_2–$FeSe_2$-CSS sample; **f** high-magnification FE–SEM image of the GW@FeS_2–$FeSe_2$-CSS sample Reproduced with permission from Ref. [106] Copyright © 2019, Royal Society of Chemistry; **g** SEM images of FeS_2@CS-40 material Reproduced with permission from Ref. [107] Copyright © 2019, American Chemistry Society; **h** low-resolution SEM and **i** high-resolution SEM images of the FeS foams with surface-grown carbon nanotube arrays Reproduced with permission from Ref. [108] Copyright © 2020, Royal Society of Chemistry

flower-like FeS_2 clusters and the stable, conductive network of 3D interlinked GA during the charge–discharge cycles.

Morteza et al. [106] introduced a new method to construct a graphene-wrapped FeS_2–$FeSe_2$ core–shell cratered sphere (GW-FeS_2–$FeSe_2$-CSS) as an anode electrode for asymmetric superconductors. This innovative construction led to notable enhancements in performance, as shown in Fig. 7e and f. Similarly, Xia et al. [109] synthesized a hierarchical heterostructure by anchoring Fe_2O_3 nanospheres onto FeS_2 nanosheets through a one-step hydrothermal treatment method. This hybrid electrode design effectively enhances the electrochemical performance. Qiao et al. [107] presented a distinct fabrication technique involving a magnetic field-guided interface coassembly to create a uniform carbon-coated FeS_2 (FeS_2@C) nanochain material. Initially, Fe_3O_4 nanospheres are assembled into chains during a polymer coating process within a dynamic magnetic field. This step is followed by successive carbonization and sulfidation treatments to generate the final FeS_2@C, as shown in Fig. 7g. The surrounding carbon layer protects the FeS_2 from degradation during electrocatalysis and augments catalytic efficiency through the interfacial interaction between metal nanoparticles and nanocarbon. Moreover, Wang et al. [108] outlined a comprehensive yet simple strategy to obtain metal sulfide (Ni_3S_2, Co_9S_8, and FeS) foams. This process entails an in situ conversion of commercial nickel (Ni), cobalt (Co), and iron (Fe) foams through a conventional annealing reaction. Interestingly, this method also facilitates the growth of nitrogen (N)-doped carbon nanotubes on the foam surfaces, which are catalyzed by the corresponding metal sulfide nanocrystals. The low- and high-resolution SEM images shown in Fig. 7h and i reveal the FeS foams adorned with carbon nanotube arrays, indicating their potential as effective electrodes in electrochemical applications. These studies underscore the significant impact of 3D morphologies in boosting IBS performance.

IBS for Supercapacitors

IBS amalgamation with other compounds can significantly enhance their properties and functionalities. The development of composite materials by combining IBSs with various structural carbons, metal compounds, and polymers can lead to improved electrical conductivity and electron transport characteristics, consequently enhancing their electrochemical energy storage properties. Furthermore, these composite formations can refine the surface properties of IBSs and increase the number of active sites available for electrochemical reactions. This not only enhances the performance but also ensures greater stability and durability, extending the long-term operational stability of IBSs across diverse applications. Table 1 summarizes the enhanced electrochemical properties of IBSs resulting from the implementation of various composite strategies.

Table 1 Performance collection of IBSs in supercapacitors under different composite strategies

Support	Structure		Electrolyte	Performance (three-electrode system)				Performance (two-electrode system)				References
	Material	Nanostructure		Voltage window	Specific surface area (SSA)	Specific capacitance	Cyclability (cycles, current density)	Rate performance	Voltage window	Maximum energy density (Maximum power density)	Cycling performance (cycles, current density)	
Carbonaceous materials	FeS/RGO (graphene oxide)/FeS@Fe	Nanosheets	2 mol/L KOH	− 1.4 V to − 0.2 V	–	247.5 C/g (206.25 F/g) at 20 mA/cm^2	118% (5000 cycles, 50 mA/cm^2)	48.5% (20 to 150 mA/cm^2)	0 to 1.8 V	34.07 Wh/kg (2666.67 W/kg)	90% (3000 cycles, 50 mA/cm^2)	[110]
	FeS/C	Nanoparticles	2 mol/L KOH	–1.4 to –0.2 V	–	275.65 F/g at 30 mA/cm^2	90% (1000 cycles, 30 mA/cm^2)	39.9% (20 to 150 mA/cm^2)	0 to 1.8 V	40.96 Wh/kg (19,600 W/kg)	90% (2500 cycles, 50 mA/cm^2)	[85]
	RGO/FeS	Nanosheets	2 mol/L KOH	− 1.3 to − 0.4 V	–	900 mF/cm^2 (300 F/g) at 10 mA/cm^2	97.5% (2000 cycles, 30 mA/cm^2)	33.3% (10 to 100 mA/cm^2)	0 to 1.9 V	27.91 Wh/kg (2093.18 W/kg)	165.0% (10,000 cycles, 30 mA/cm^2)	[111]
	FeS/carbon nanofiber	Nanoparticles on nanofiber	6 mol/L KOH	− 1.2 to − 0.2 V	–	503 F/g at 2 A/g	90% (1000 cycles, 2 A/g)	80% (2 to 10 A/g)	–	–	–	[88]
	2D-ZFS@CC	Nanosheets	6 mol/L KOH	− 1.4 to 0.0 V		1367.5 F/g (1641 C/g) at 3 A/g	87% (5000 cycles, 15 A/g)	58.5% at ten-fold high current density	–	–	–	[112]
	N/S codoped carbon nanofibers (FeS_2CNFs)	Nanofibers	6 mol/L KOH	− 1.2 to − 0.2 V	200.17 m^2/g	511 F/g at 1 A/g	94.5% (5000 cycles, 1 A/g)	76.4% (1 to 5 A/g)	0 to 1.6 V	73.3 Wh/kg (800 W/kg)	490.6 mAh/g after 200 cycles at 500 mA/cm^2	[113]
	GA-FeS_2	Nanoflowers	6 mol/L KOH	− 0.9 to − 0.3 V	8.39 m^2/g	331.6 F/g at 0.5 A/g	88.2% (2000 cycles, 10 A/g)	55.2% (0.5 to 10 A/g)	–	22.86 Wh/kg (400.0 W/kg)	96.2% (3000 cycles,)	[103]
	$Fe_{1-x}S$-TiO_2/CNFs	Nanofibers	2 mol/L KOH	0 to 0.5 V	291.06 m^2/g	138 F/g at 1 A/g	83% (2000 cycles, 5 A/g)	68.7% (1 to 5 A/g)	–	–	–	[114]
	FeS_x/C/CNT	Nanosphere	3 mol/L KOH	− 1.2 to − 0.4 V	–	617.5 F/g at 1 A/g	–	59.1% (1 to 5 A/g)	–	–	–	[115]
	GCN/Fe_3S_4	Nanoparticles	6 mol/L KOH	0.1 V to 0.6 V	–	104 F/g at 1 A/g	92% (10 000 cycles, 5 A/g)	72% (1 to 25 A/g)	–	9.4 Wh/kg (0.8 kW/kg)	–	[83]
	FeS_2/GNS	Nanoparticles on graphene nanosheets	2 mol/L KOH	− 1.1 to 0 V	135 m^2/g	793 C/g at 3 A/g	85% (2500 cycles, 20 A/g)	82% (3 to 30 A/g)	0 to 1.7 V	95.8 Wh/kg (949 W/kg)	86% (5000 cycles, 15 A/g)	[116]

Table 1 (continued)

Support	Structure		Electrolyte	Performance (three-electrode system)				Performance (two-electrode system)				References
	Material	Nanostructure		Voltage window	Specific surface area (SSA)	Specific capacitance	Cyclability (cycles, current density)	Rate performance	Voltage window	Maximum energy density (Maximum power density)	Cycling performance (cycles, current density)	
Other metal compounds	Fe_3O_4@FeS	Nanosheets	3 mol/L KOH	−1.2 to 0.2 V	–	703.9 F/g at 1 A/g	80.2% (10,000 cycles, 10 A/g)	70.6% (1 to 20 A/g)	0 to 1.6 V	64.6 Wh/kg (800 W/kg)	79.5% (5000 cycles, 10 A/g)	[117]
	FeS thin film	Nanoparticles on thin film	2 mol/L KOH	−0.2 V to 0.6 V		36.6 mF/cm^2 at 0.15 mA/cm^2	89% (5000 cycles, 0.7 mA/cm^2)	55% (5 to 100 mA/s)	0 to 1.7 V	7.28 mWh/cm^3 (6.4 W/cm^3)	91% (14,000 cycles, 8.0 mA/cm^2)	[94]
	FeS nanoflakes thin film	Nanoflakes on thin film	1 mol/L $LiClO_4$	0 to 1.2 V		297 F/g at 0.8 mA/cm^2	90% (1000 cycles, 100 mV/s)	65.0% (0.8 to 2.4 mA/cm^2)	0 to 2 V	2.56 Wh/kg (726 W/kg)	91% (1000 cycles, 100 mV/s)	[118]
	Diatomite-like $KFeS_2$	Diatomite-like	6 mol/L KOH	0 to 0.45 V	42.35 m^2/g	651 F/g at 1.0 A/g	–	66.8% (1 to 10 A/g)	–	–	–	[97]
	Flaky FeS/nitrogen-doped defective reduced graphene oxide	Flake-like morphology with hierarchical porosity	2 mol/L KOH	−1.2 to 0 V	88 m^2/g	393 F/g at 10 mV/s	–	–	–	–	–	[119]
	FeS/NF coral reef-like nanostructure	Coral reef-like nanorods	2 mol/L KOH	0 to 0.45 V	–	2007.61 F/g at 2 A/g	97% (3000 cycles, 2 A/g)	52.27% (2 to 20 A/g)	–	54.88 Wh/kg (500 W/kg)	–	[120]
	Fe_2O_3/FeS-decorated N, S-codoped hierarchical porous carbon hybrid	Nanosheet	6 mol/L KOH	–0.9 to 0.3 V	658.5 m^2/g	1320.4 F/cm^3 at 0.1 A/g	100% (50,000 cycles, 80 A/g)	76.4% (10 to 80 A/g)	–	100.9 Wh/kg (221.9 Wh/L)	–	[121]
	$FeCo_2S_4$–$NiCo_2S_4$	Nanotubes	3 mol/L KOH	0 to 0.6 V	–	1519 F/g at 5 mA/cm^2	95.1% (5000 cycles, 5 mA/cm^2)	85.1% (5 to 40 mA/cm^2)	0 to 1 V	46 Wh/kg (1070 W/kg)	92% (3000 cycles, 10 mA/cm^2)	[122]
	$FeCo_2S_4$ HNNA/CNF	Nanofibrous network	3 mol/L KOH	0 to 0.6 V	–	2476 F/g at 1 A/g	93% (5000 cycles, 10 A/g)	55% (1 to 20 A/g)	0 to 1.6 V	88.5 Wh/kg (800 W/kg)	81.2% (5000 cycles, 4 A/g)	[87]
	$FeCo_2S$	Nanoflakes	1 mol/L KOH	–0.1 to 0.45 V	–	827.5 F/g at 1 A/g	93.2% (5000 cycles, 5 A/g)	84.1% (1 to 10 A/g)	0 to 1.3 V	67.8 Wh/kg (1.6 kW/kg)	84.1% (4000 cycles, 6.5 A/g)	[123]
	$NiFeS_x$@CNTs@MnS@Diatomite	Diatomite-like	6 mol/L KOH	0 to 0.4 V	62.3 m^2/g	552 F/g at 1 A/g	89.8% (5000 cycles, 5 A/g)	68.4% (1 to 10 A/g)	0 to 1.5 V	28.9 Wh/kg (9375 W/kg)	88.03% (5000 cycles, 5 A/g)	[124]
Polymers	FeS_2/PVP/NF (polyvinyl pyrrolidone)	Nanosheets	3 mol/L KOH	−1.0 to 0.5 V	–	526.08 F/g at 1 A/g	91.2% (3000 cycles, 1 A/g)	48.82% (1 to 10 A/g)	–	–	–	[18]

IBSs Nanocomposites Consist of Carbonaceous Materials

Owing to their superior electrical conductivity, large SSA, affordability, and structural controllability, carbon materials such as graphene quantum dots, carbon nanotubes, graphene, and porous carbon have garnered significant attention in energy storage and conversion [125–128]. Consequently, IBS amalgamation with various dimensional carbon frameworks not only addresses the inherent low electrical conductivity but also modulates the morphology of IBS crystals, facilitating improvements in reaction kinetics, rapid charge/discharge rates, and cycling stability of IBS materials/carbon composites [129]. A comparison of the physicochemical properties of carbon materials of different dimensions is depicted in Fig. 8. To ameliorate the low electrical conductivity of IBS materials and augment their SSA and active sites, composite formation with conductive carbon skeletons or structural carbon is deemed an efficacious solution to the aforementioned challenges [130]. This section will review recent advancements in IBS/carbon hybrid electrodes, elucidating their advanced properties in terms of structural design strategies and the resultant properties attained.

Carbon materials such as carbon dots, carbon nanofibers, carbon nanotubes, and graphene/graphene oxides exhibit high electrical conductivity, good flexibility, and superior functionality, making them widely used as single-electrode materials or conductive substrates for superconductors. In this process, IBSs are physically or chemically introduced in situ onto the carbon surface, or the carbon is grown on the IBS surface. This strategy effectively controls the IBS morphology while significantly improving overall electrical conductivity, power density, and energy density. Zhao et al. [115] prepared a new type of FeS_x/C/CNT composite with micro-sized spherical particles via spray drying and subsequent high-temperature calcination in an inert atmosphere, as shown in Fig. 9a. The morphology of FeS_x/C/CNT is depicted in Fig. 9b and c. SEM images at low magnification reveal that the composite comprises primary nanoparticles, amorphous carbon, and stacked carbon nanotubes. Elemental mapping of FeS_x/C/CNT, C, Fe, and S is uniformly distributed, mainly concentrated on the spherical particles, suggesting that FeS_x in FeS_x/C/CNT is well wrapped by C/CNT, thus providing a good conductive skeleton. The specific capacitances of the FeS_x/C/CNT composites were measured at 617.5, 508.0, 436.1, and 365.0 F/g at current densities of

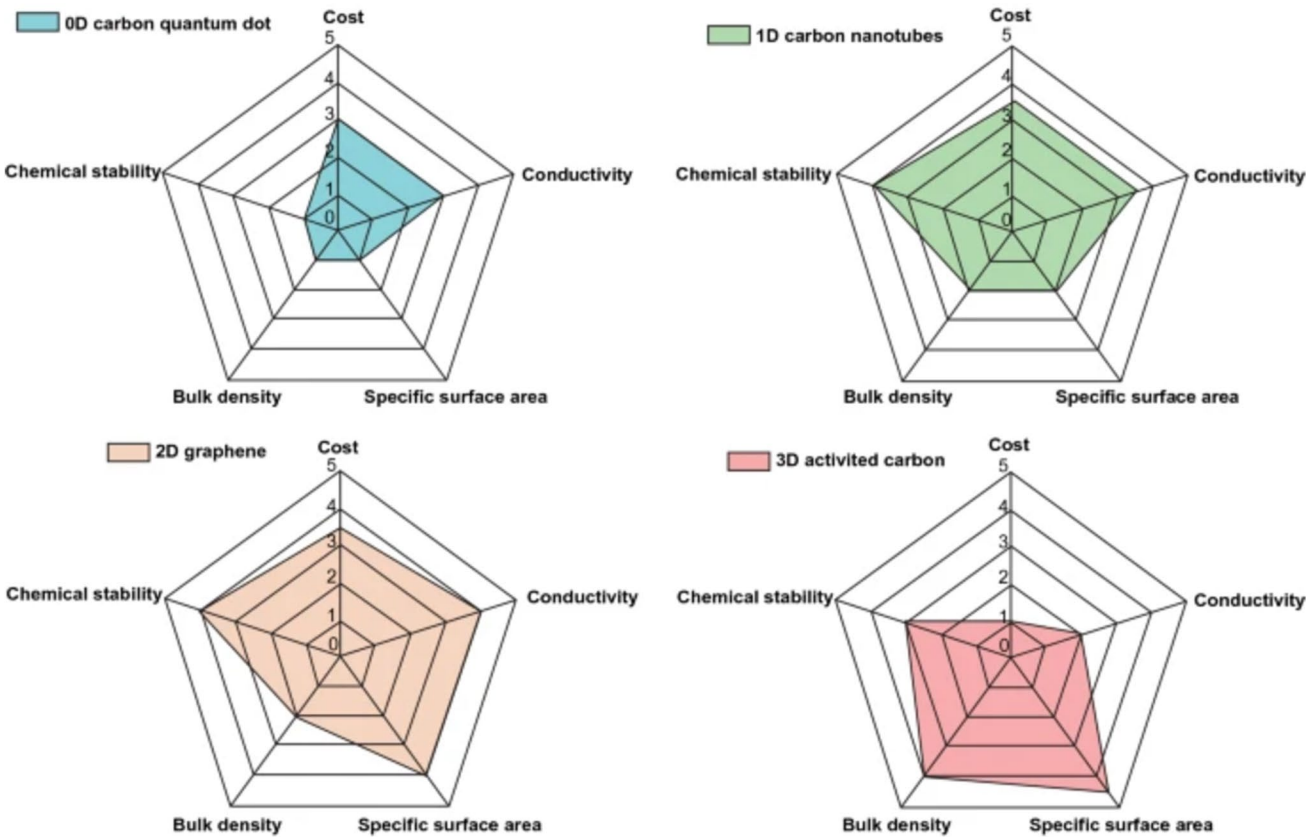

Fig. 8 Comparison of the physicochemical properties of different carbon dimensions Reproduced with permission from Ref. [130]. Copyright © 2021, Springer Nature

1, 2, 3, and 5 A/g, respectively, highlighting their potential as high-performance superconductor electrode materials. Sun et al. [116] synthesized FeS_2 nanoparticles anchored on graphene nanosheets (FeS_2/GNS) with integrated electrochemical properties using a facile and rapid microwave-assisted hydrothermal method, as shown in Fig. 9d. SEM images of pristine FeS_2 and FeS_2@HPC are presented in Fig. 9e and f. The FeS_2/GNS anodes exhibited a high specific capacity of up to 793 C/g at 3 A/g, surpassing commonly used carbon and metal oxide anodes. The anode material also exhibited excellent multiplicative capability (82% capacity at 30 A/g) and impressive cycling stability (88% capacity retention after 5000 cycles at 20 A/g). Subsequently, a FeS_2/GNS// $Ni(OH)_2@Co_9S_8$ solid-state hybrid supercapacitor device was assembled. Owing to the perfect matching of the anode and cathode, the system voltage was extended to 1.7 V. With the high specific capacity and wide potential range of the FeS_2/GNS anode, the hybrid supercapacitor achieved a high-energy density of 95.8 Wh/kg at an average power density of 949 W/kg. Furthermore, this all-solid-state hybrid device demonstrated robust cycling stability, retaining 86% of its capacitance after 5000 cycles.

Xu et al.[131] successfully synthesized FeS_2 nanocrystals@hierarchical porous carbon (HPC) using pre-prepared HPC. After 100 cycles, the specific capacity of FeS_2@HPC reached 720 mAh/g (Fig. 9g). This high capacity is attributed

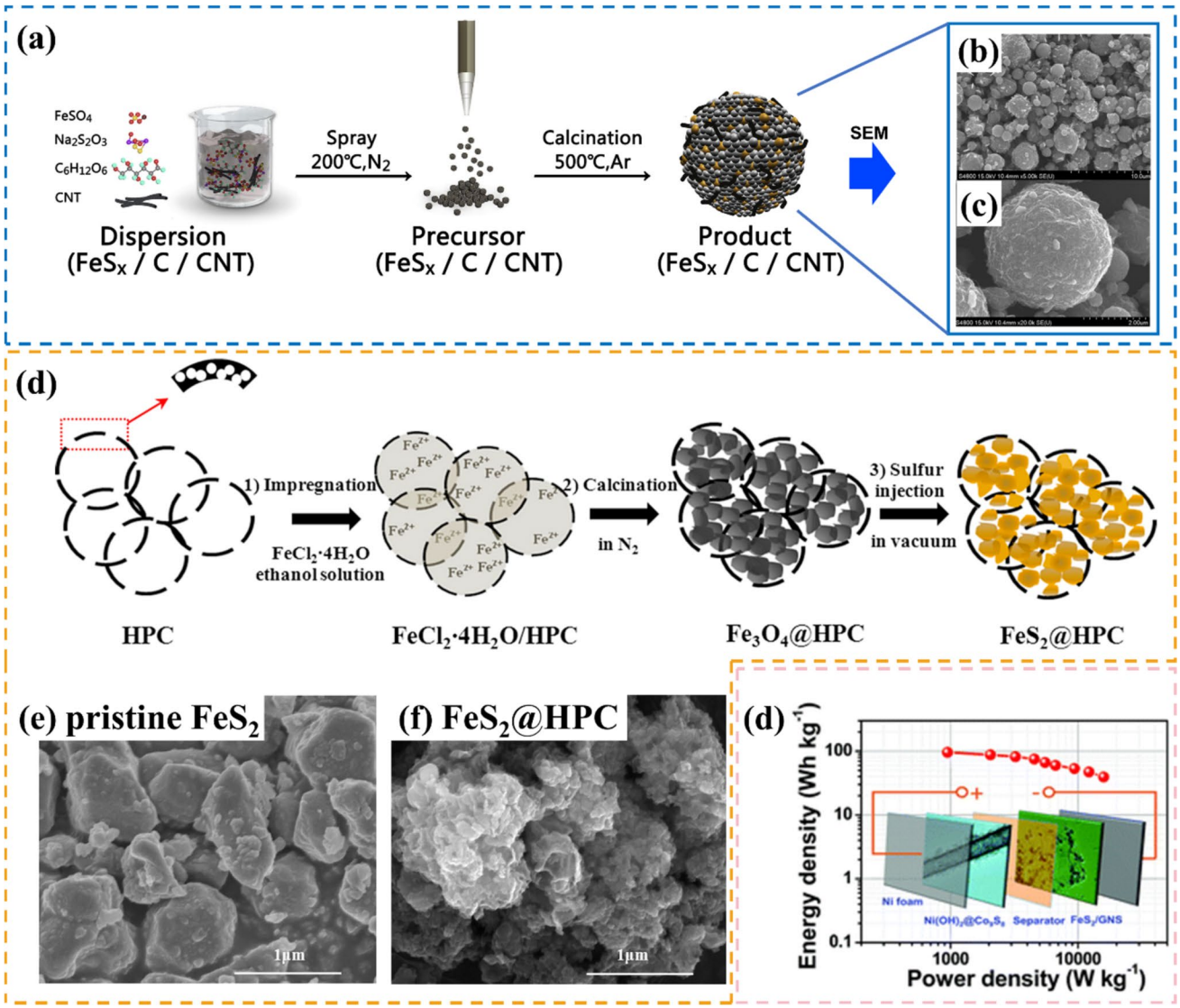

Fig. 9 **a** Schematic diagram of preparation of FeS_x/C/CNT; **b, c** SEM images of FeS_x/C/CNT Reproduced with permission from Ref. [115]. Copyright © 2020, Elsevier; **d** Formation process of FeS_2 nanocrystals in hierarchical porous carbon capsules; SEM images of **e** pristine FeS_2 and **f** FeS_2@HPC Reproduced with permission from Ref. [116]. Copyright © 2018, Elsevier; **g** schematic diagram of the FeS_2/GNS performance and capacitor structures Reproduced with permission from Ref. [131]. Copyright © 2016, Elsevier

to the HPC's interconnected macroporous carbon capsule and microporous shell, which effectively buffer the volume changes in FeS_2, restrain FeS_2 growth to nanoscale particles, and inhibit the loss of active substances during cycling. Zhao et al. [132–134] synthesized a porous RGO/FeS composite in situ on the Fe foil surface. This RGO/FeS was directly used as a supercapacitor electrode, exhibiting excellent electrochemical performance: 900 mF/cm^2 (300 F/g) with 97.5% maximum capacity retention after 2000 cycles. The impressive performance is attributed to graphene's role as a soft, flexible support that alleviates volume changes, increasing cyclability, and improving the composite conductivity. Additionally, graphene's high SSA allows for uniform anchoring of active material particles, preventing agglomeration and controlling particle size [135]. Huang et al. [87] reported the rational design and synthesis of a novel flexible supercapacitor electrode consisting of lawn-like $FeCo_2S_4$ hollow nanoneedle arrays ($FeCo_2S_4$ HNNA) grown on electrospun carbon nanofiber film via a two-step sulfidation method. In this setup, the porous carbon nanofiber film induces homogeneous nucleation of $FeCo_2S_4$ nanoneedles, provides fast charge transfer pathways during electrochemical processes, and acts as a robust current collector for binder-free electrodes. This design results in excellent material performance, manifesting a high specific capacitance of 2476 F/g at 1 A/g and delivering a high-energy density of 88.5 Wh/kg at 800 W/kg, as well as excellent cycling stability, retaining 81.2% of its capacitance after 5000 charge/discharge cycles.

IBS Nanocomposites Consist of Other Metal Compounds

The compositing of IBSs with other metal compounds is a widely used method for enhancing the electrochemical properties of IBS materials. Li et al. [124] demonstrated the synthesis of a novel 3D multi-component structure composed of sulfated NiFe LDH ($NiFeS_x$@CNTs@MnS@diatomite) nanosheets and carbon nanotubes on diatomite using the chemical vapor deposition and hydrothermal methods (Fig. 10a). The addition of carbon nanotubes improved the nanomaterial morphology, as illustrated in Fig. 10b and c, and reduced its electrochemical impedance, resulting in an excellent conductive material with shortened electron transfer and ion diffusion paths. This material exhibited a capacitance of 552 F/g at 1 A/g, a rate capacity retention of 68.4% at 10 A/g, and a capacitance retention of 89.8% after 5000 cycles. Furthermore, it demonstrated a maximum energy density of 28.9 Wh/kg and a maximum power density of 9375 W/kg in a two-electrode test. Another approach for enhancing electrochemical performance involves combining active components and conductive substrates, which reduces internal resistance and provides excellent cycling stability [136, 137]. Hao et al. [80] devised a high-energy density hybrid supercapacitor (HSC) utilizing FeS_2/CoS_2 @KC-800 as the cathode and NSKC-800 as the anode. The integration of metal disulfides and conductive porous carbons effectively alleviates volume expansion during charge/discharge cycles, thereby improving overall electrochemical performance. The obtained FeS_2/CoS_2 @KC-800 exhibited a high specific capacitance of 3480.47 F/g at 0.5 A/g and retained 2100.38 F/g at 15 A/g. In a different study, Ma et al. [93] synthesized 3D sulfur-doped graphene loaded with Ni–Fe bimetallic sulfides via a one-step microwave aluminothermic method using TGA as the sulfur source. The small particle size of the Ni–Fe sulfide, combined with the spatial network structure of the 3D graphene, provided an increased contact area between the electrode and the electrolyte, resulting in a specific capacitance of 643.9 C/g (1073.2 F/g) at a current density of 1 A/g in a 6.0 mol/L KOH electrolyte. Furthermore, the asymmetric supercapacitor device composed of $NiFeS_2$/3DSG electrodes as the positive electrode and 3DSG as the negative electrode ($NiFeS_2$/3DSG//3DSG) showcased a superior energy density of 45.7 Wh/kg at a power density of 222 W/kg over a wide potential range of 1.6 V. The device retained 82% of its specific capacitance after 5000 charge/discharge cycles. Additionally, Huang et al. [87] designed and synthesized a flexible supercapacitor electrode consisting of a lawn-like $FeCo_2S_4$ hollow nanopin array ($FeCo_2S_4$ HNNA) on a carbon nanofiber film utilizing a two-step vulcanization method. Tao et al. [138] employed a solvothermal process (Fig. 10d) followed by reduction with $NaBH_4$ to prepare reduced graphene oxide-based $FeNi_2S_4$ electrode materials with abundant sulfur vacancies (r-$FeNi_2S_4$-rGO) as shown in Fig. 10e and f. This structure achieved excellent performance, suggesting a fast reversible property for the capacitor (Fig. 10g). The performance enhancement mechanism is shown in Fig. 10h: rGO with continuous channels acts as a conducting base to shorten the electron transfer path. Sulfur vacancies, acting as siderophore defects, facilitate electron jumping between metal ions, increasing siderophore density and improving conductivity. At the same time, sulfur vacancies provide additional active sites that improve the adsorption capacity of OH– and accelerate redox reaction kinetics.

IBSs Nanocomposites Consisting of Polymers

The combination of IBSs and conductive polymers is also a very common modification method. Conductive polymers, such as polypyrrole, polyaniline, and polythiophene, are considered are considered highly promising materials for pseudocapacitors in supercapacitors owing to their excellent conductivity, low cost, and ease of synthesis [139–143]. In general, a high-performance electrochemical electrode requires minimizing four primary resistances during electrochemical charge–discharge: (1) ion transport in the

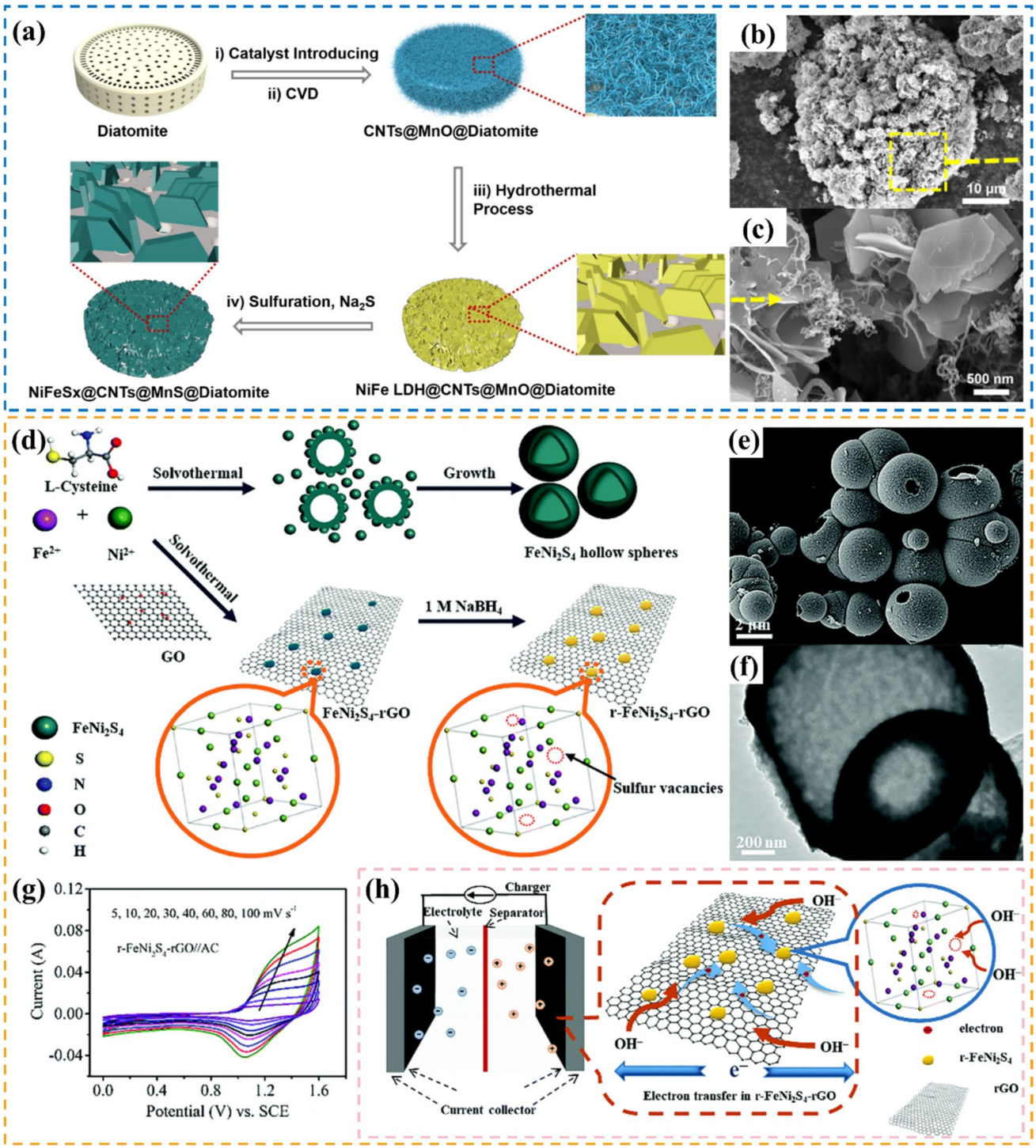

Fig. 10 **a** Schematic illustration for the preparation process of $NiFeS_x$@CNTs@MnS@Diatomite; **b, c** SEM images in different scales of $NiFeS_x$@CNTs@MnS@Diatomite Reproduced with permission from Ref. [124]. Copyright © 2021, Elsevier; **d** illustration of the synthesis process of $FeNi_2S_4$, $FeNi_2S_4$-rGO, and r-$FeNi_2S_4$-rGO; **e** FESEM image and **f** TEM image of $FeNi_2S_4$ hollow spheres; **g** CV curves at different scan rates; **h** Schematic illustration of the possible mechanism of the r-$FeNi_2S_4$-rGO electrode for energy storage in an alkaline electrolyte Reproduced with permission from Ref. [138]. Copyright © 2021, Royal Society of Chemistry

electrolyte; (2) ion transport in the electrode; (3) electrochemical reactions in the electrode; and (4) electron conduction in the electrode and current collector (Fig. 11a). Lee et al. [144] achieved good reversibility and efficiency by embedding pure natural cubic FeS_2 (pyrite) in a stabilized polyacrylonitrile (PAN) matrix. The PAN matrix restricts the electrically active reduced species of FeS_2 and traps intermediate polysulfides and elemental iron, preventing them from dissolving into the electrolyte when fully charged, as shown in Fig. 11b–d. In addition to this, there are still few studies on the composite of IBSs with conductive polymers for superconductor electrodes, requiring further research to exploit more IBS properties [140, 145, 146].

Moreover, since conductive additives are not mechanically bound, they tend to aggregate upon volume expansion, disrupting the electrical connection, as shown in Fig. 11e. By contrast, nanostructured conductive polymers can be practically applied to high-capacity alloy-type anodes owing

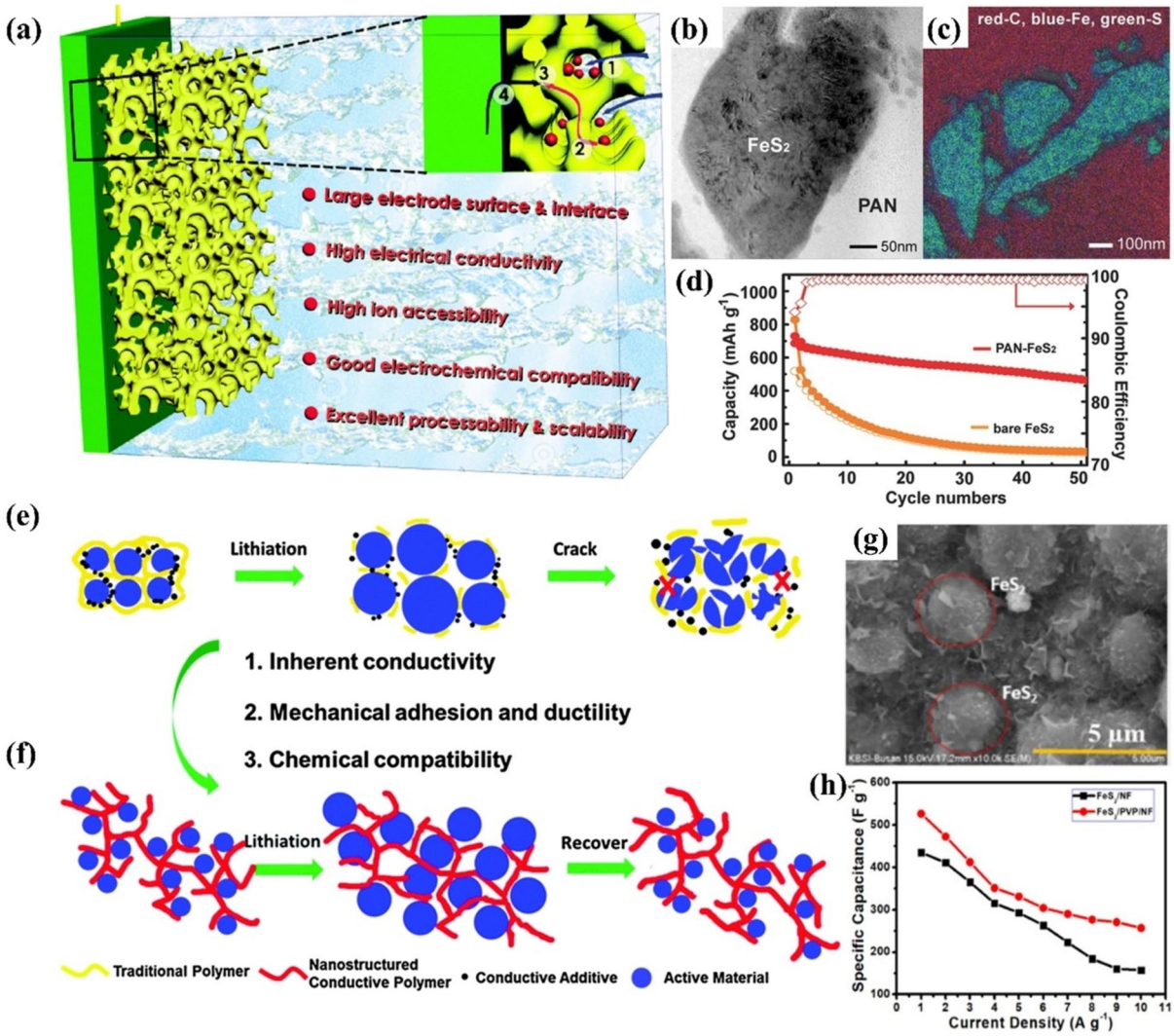

Fig. 11 **a** Schematic representation of a high-performance electrolyte electrode with the following desirable properties: large electrode surface and interface, high electrical conductivity, high ionic accessibility, good electrochemical compatibility, and excellent processability and scalability. The enlarged image illustrates the four main resistances in the electrode Reproduced with permission from Ref. [143]. Copyright © 2022, Elsevier; **b** TEM image of an embedded FeS_2 particle in a PAN-FeS_2 electrode collected after completing its 10th charge; **c** EELS elemental mapping of C (red), Fe (blue), and S (green); **d** cyclic stability of the stabilized PAN-FeS_2 electrode versus that of a bare FeS_2 electrode. Specific capacity is reported concerning the mass of the FeS_2 active material Reproduced with permission from Ref. [144]. Copyright © 2014, Wiley; **e** Traditional approach using a conductive additive and a polymer as a mechanical binder may result in broken electric contacts; **f** a nanostructured conductive polymer, which plays multiple functions, as a conductor and a binder, could maintain both electrical and mechanical integrity of the electrode during cycling Reproduced with permission from Ref. [143]. Copyright © 2022, Elsevier; **g** FE–SEM images of FeS_2/PVP material on Ni foam; **h** specific capacitance vs current density curve for FeS_2/PVP/NF Reproduced with permission from Ref. [18]. Copyright © 2020, Elsevier

to their unique properties, as shown in Fig. 11f: (1) excellent electronic conductivity inherited from the conductive polymer framework; (2) robust mechanical adhesion and ductility to withstand large volume changes; and (3) high ionic conductivity facilitated by good electrolyte absorption [143]. A considerable amount of research has focused on developing self-supporting and binder-free electrode materials for supercapacitor applications. Typically, discrete powdered materials are mixed or blended with conductive agents such as carbon black and insulating polymer binders such as polytetrafluoroethylene and polyvinylidene oxide to synthesize electrodes. However, the addition of binders and conductive agents increases polarization, dead volume, and self-weight of the electrode, which negatively impacts rate performance. Therefore, exploring new polymeric binder materials compounded with iron-sulfide agents is key to ameliorating the above-mentioned problems [147, 148]. Recently, Kim et al. [18] successfully deposited FeS_2/PVP on Ni foams via a chemical bath deposition method, as shown in Fig. 11g. This process leveraged the complementary properties of FeS_2 and PVP's considerable surface area, alongside its high thermal and mechanical conductivity, to fabricate high-performance electrodes for supercapacitors. This pioneering study is the first to employ FeS_2/PVP/NF for supercapacitor applications. The FeS_2/PVP/NF composites exhibited various advantages, such as enhanced reversible capacity, improved rate capability, and greater cycling stability owing to the presence of PVP molecules [149]. Additionally, PVP nanoparticles exhibited multiple distinct advantages, such as expedited electronic communication, increased surface area, and minimal toxicity [150, 151]. Figure 11h presents the specific capacitance in different current densities. Therefore, this study could provide a new avenue for improving the specific capacitance performance and commercialization of FeS_2/PVP-based supercapacitors.

Optimization Strategies for IBS Electrode Materials

Enhancing the electrochemical properties of IBS materials by exploring and adjusting material defects is an effective strategy. By strategically introducing material defects to the material, several benefits can be achieved: increasing the number of active sites, facilitating charge transfer rates, and bolstering overall stability. These changes can lead to significant improvements in the electrochemical performance of these materials [152–154].

IBSs Nanocomposites Doped with Foreign Atoms

Doping foreign atoms into transition metal compounds has recently emerged as an effective method for enhancing the electrochemical properties of electrodes. This approach increases the number of active sites available for redox reactions, thereby enhancing the overall electrochemical performance [155–158]. Ni, S, and phosphorus (P) are commonly used elements owing to their appropriate electronegativity and atomic radius. When N, S, or P are introduced, they formed new bonds are formed with other atoms, causing lattice distortion and changes in chemical characteristics. For example, Huang et al. [113] synthesized FeS_2CNFs doped with N and S, as shown in Fig. 12a. They used a hydrothermal method to prepare hollow Fe_2O_3 nanospheres, which were then mixed with PAN to form Fe_2O_3/PAN precursors through electrospinning. These precursor films were subsequently pre-oxidized and calcined at 500 °C in N_2 atmosphere to obtain Fe_3O_4CNFs. The Fe_3O_4CNFs were then sulfur doped in situ at 400 °C in an argon atmosphere to produce FeS_2CNFs, as shown in Fig. 12b–d. Additionally, Qu et al. [159] designed and synthesized porous P-doped FeS_2 nanoparticles supported on graphene nanosheets (P–FeS_2/GNS, referred to as PFSG) composite. The synthesis process of PFSG, as shown in Fig. 12e, involved first growing FeS_2 on graphene oxide using an ultrafast microwave method (FSG). P was then doped into FSG through a heating treatment. During this process, the P source ($NaH_2PO_2{\cdot}H_2O$) releases PH_3 gas, which reacts with water on the FSG surface to form a porous architecture. This unique structure facilitates rapid electrolyte ion diffusion during electrochemical testing. Figure 12f, g shows that the FeS_2 retains its flower-like structure post-phosphorous doping. The PFSG morphology differs significantly from that of pristine P–FeS_2, as shown in Fig. 12h–j. PFSG displays a loose structure with numerous P–FeS_2 nanoparticles uniformly distributed on graphene nanosheets (Fig. 12h), effectively preventing graphene aggregation (Fig. 12i and j). As expected, the resulting porous PFSG composite shows high performance as an anode for supercapacitors, holding great potential for application in high-performance energy storage systems.

Vacancies in IBSs Nanocomposites

Vacancies are currently the most prominent method used to improve electrode performance in IBSs. Other material defects have received limited research attention [160–163]. Thus, this section will mainly review methods that utilize vacancies to enhance IBS performance. Qian et al. [164] rationally designed FeS_2 microflowers with sulfur vacancies through in situ P doping, which induced atomic rearrangement and the introduction of P atoms. This special structure, as shown in Fig. 13a, contained a large number of nanoparticles and organic-derived carbon (Fig. 13b and c), effectively reducing volume expansion and maintaining structural stability. The atomic rearrangement and sulfur vacancies also adjusted the electronic structure, improving

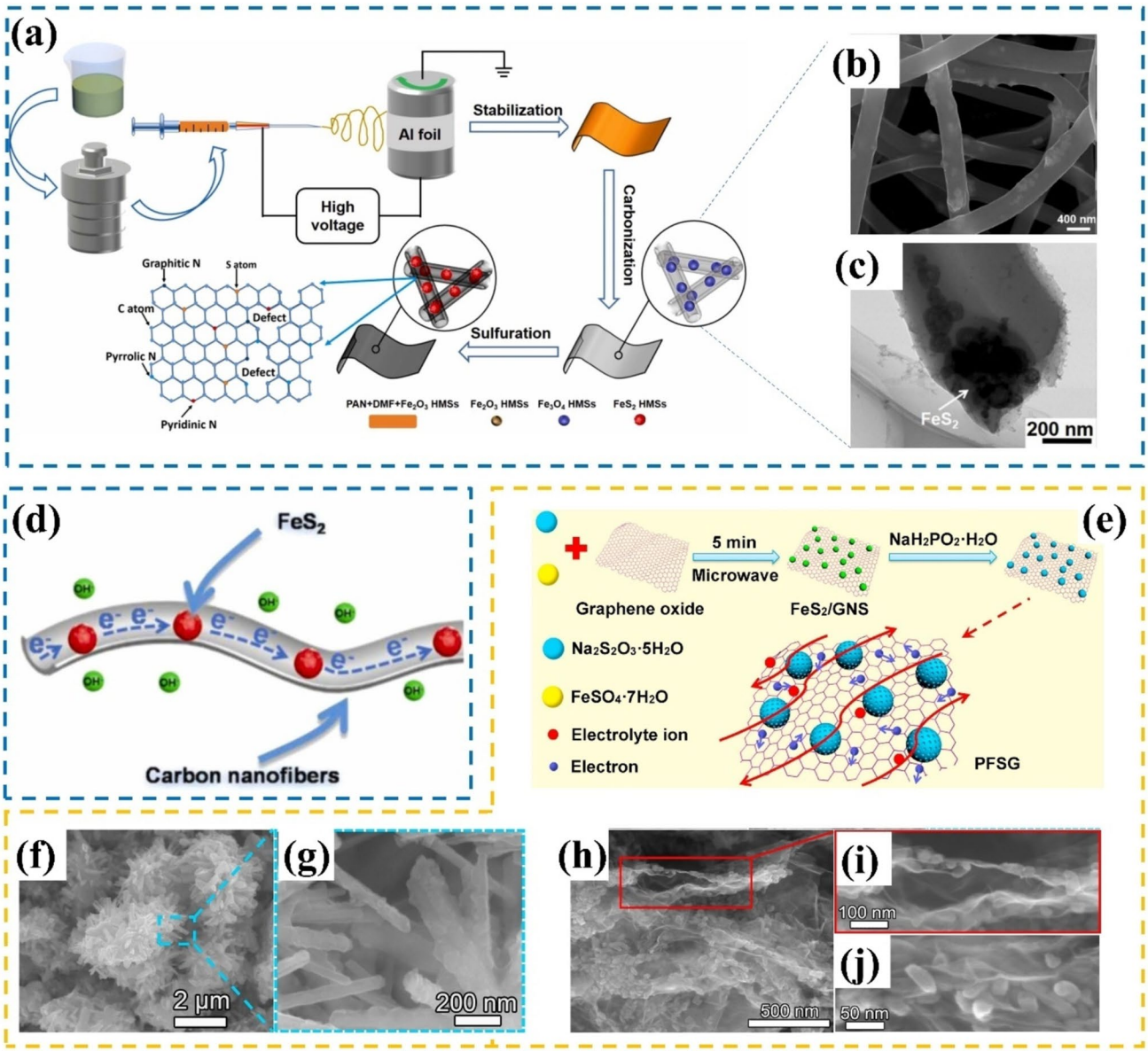

Fig. 12 **a** Illustration of the preparation procedure for FeS_2CNFs; **b** FESEM images of FeS_2CNFs; **c** HRTEM of a single particle of FeS_2CNFs; **d** schematic diagram of fast charge transfer and ion diffusion at the FeS_2CNFs electrode in Faradic redox reaction Reproduced with permission from Ref. [113] Copyright © 2022, Elsevier; **e** schematic diagram of the synthesis process for the PFSG; SEM images of **f, g** P–FeS_2 and **h–j** PFSG [159] Reproduced with permission from Ref. [159] Copyright © 2022, Elsevier

conductivity, increasing the number of active sites, and enhancing overall electrochemical performance. In another study by Qian et al. [165], sulfur vacancies were quantitatively increased in FeS_2 nanorods as anode materials, thereby significantly improving their energy storage performance. The synthesis process of these FeS_2 nanorods and the resulting product are illustrated in Fig. 13d–g, respectively. Sulfur defects effectively provided electron donors, reduced the jump energy barrier for conduction and valence band electrons, and enhanced conductivity. Deng et al. [166] further explained the enhancement mechanism of sulfur vacancies in FeS_2 through adsorption spectrum analysis. The structural features of FeS_2 and the calculated adsorption coefficient of FeS_2 with sulfur vacancies demonstrated improved electrical conductivity and photocatalytic properties of the FeS_2 electrode material. Hence, the introduction of sulfur vacancies effectively increases IBS conductivity, leading to improved electrochemical performance of the electrode by increasing the number of active sites [167–172].

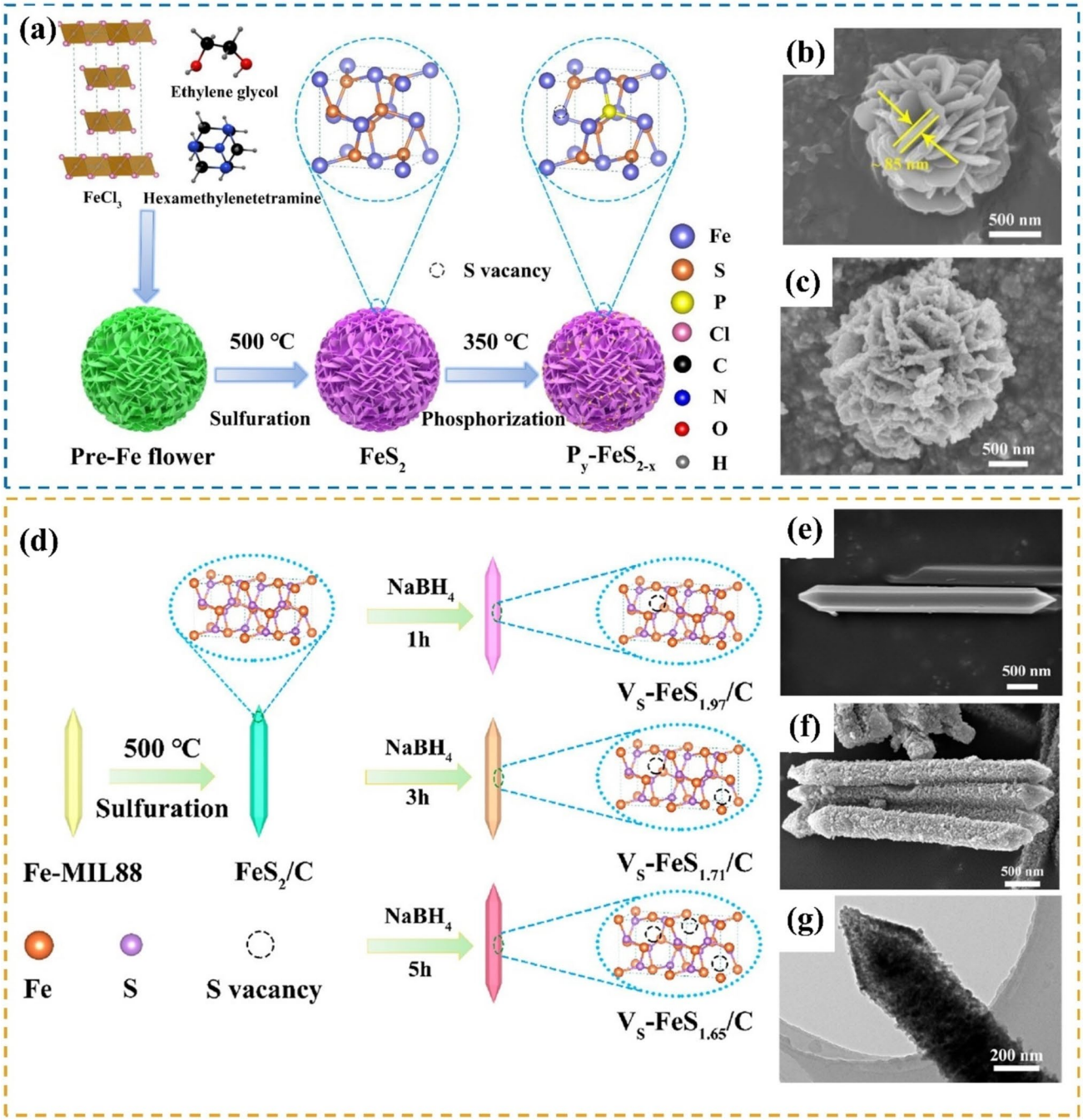

Fig. 13 **a** Schematic illustration of the fabrication process of the P_y-FeS_{2-x} microflowers.; ESEM images of **b** Pre-Fe flower and **c** $P_{1.0}$-FeS_{2-x} microflower Reproduced with permission from Ref. [164]. Copyright © 2022, Elsevier; **d** schematic illustration of the synthesis process of the V_S-FeS_{2-x}/C nanorods; FESEM images of **e** Fe-MIL88 nanorods and **f** V_S-$FeS_{1.71}$/C nanorods; **g** TEM image of V_S-$FeS_{1.71}$/C nanorods Reproduced with permission from Ref. [165]. Copyright © 2022, American Chemistry Society

Conclusion and Perspective

In this paper, we provide a comprehensive review of strategies aimed at mitigating the primary limitations encountered by IBS composites when used as electrode materials in supercapacitors. This study focuses on recent progress in three key aspects of IBS composite nanomaterials: architectural design, material compounding, and defect modulation. By analyzing current research methodologies designed to address IBS drawbacks, this study assesses the impact of different strategies on their electrochemical properties. It covers the design and controlled synthesis of 0D–3D

nanostructures, composite formation with other materials (such as IBS nanocomposites with various carbonaceous carriers, composites with other metal ions, and polymers), and material defect engineering. Detailed analyses of selected exemplary experiments are provided.

Looking forward, recent research on IBS electrode materials for supercapacitors should address five key challenges despite their benefits. This paper outlines these challenges and links them to the IBS advantages, as depicted in Fig. 14. Additionally, the paper offers suggestions and perspectives on the next research directions from five specific aspects, aiming to inspire ideas and strategies for future research in this field.

Design New Architectures

Explore novel IBS nanostructures or discover new architectures (e.g., biomimetic morphology/templates) for material synthesis. Wang et al. [97] achieved high performance in supercapacitors by constructing biomimetic diatom structures for IBSs, demonstrating a promising avenue for enhancing electrochemical properties.

Composite Suitable Materials

Integrate IBSs with one or several other materials, such as structural carbon materials, other metal ions/compounds, and polymers, to complement their strengths and effectively improve their electrochemical properties. Li et al. [124] achieved high performance by compositing IBSs with equally high-performance materials, effectively balancing their strengths and weaknesses.

Synthesize Material Defects

Introduce material defects, such as vacancies, to modulate material properties. However, this strategy has been relatively underutilized in studies on IBS materials. Qu et al. [159] significantly improved the electrochemical performance of IBSs through P doping. Characterizing these defects using advanced techniques like aberration-corrected transmission electron microscopy, atomic force microscopy, and qualitative or quantitative analyses such as X-ray absorption fine structure and electron paramagnetic resonance spectroscopy is essential.

Understand Mechanisms of Materials Synthesis

Despite numerous new structures, composites, and material defects being synthesized, their formation mechanisms remain unclear and often rely on empirical methods. Elucidating these mechanisms underlying their formation is crucial for further enhancing and developing new composite materials. This represents a significant challenge that warrants increased focus in future research.

Investigate Mechanisms of Electrochemical Reactions

Many studies lack in-depth explanations regarding changes in electrochemical reaction mechanisms after adopting certain methods. Future research should emphasize elucidating these reaction processes and mechanisms using advanced

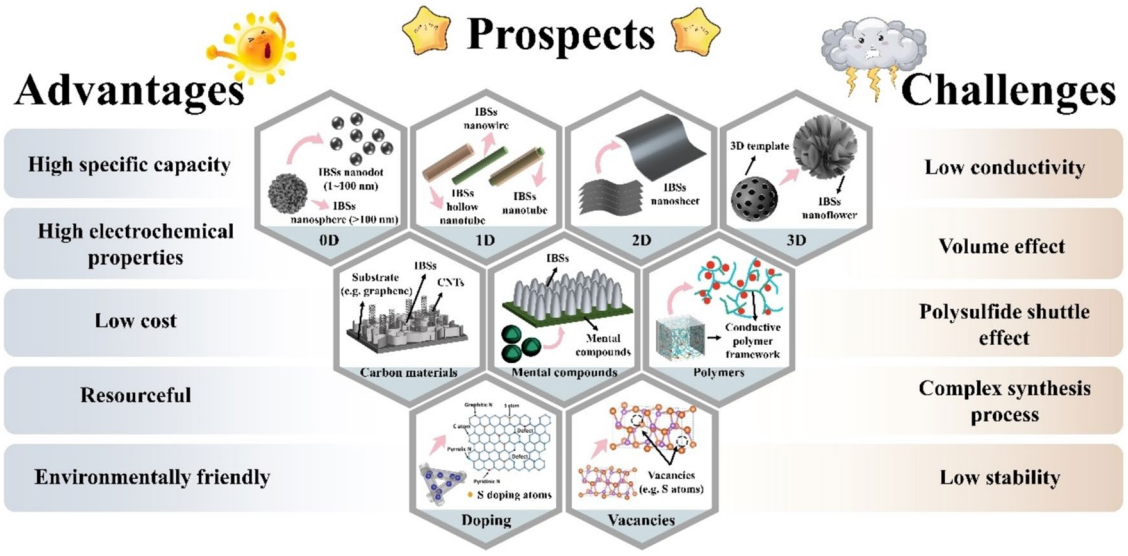

Fig. 14 Abstract of the prospects outlined in this article and the intrinsic connections between advantages and challenges

material characterization tools such as in situ X-ray diffraction, X-ray photoelectron spectroscopy, Raman spectroscopy, and Fourier transform infrared spectroscopy. Furthermore, experimental results can be corroborated and analyzed alongside density functional theory calculations to derive fundamental principles.

The advancement of IBS nanomaterials and their utilization as supercapacitor electrodes hold significant promise for the future. However, these materials are still primarily in the research stage, and numerous challenges remain to be resolved. This review of recent research progress will serve as a valuable reference for future studies in this field, thereby fostering the further development of IBSs as supercapacitor electrode materials.

Acknowledgements This work is supported by the National Natural Science Foundation of China (No. 52378217), National Training Program of Innovation and Entrepreneurship for Undergraduates (No. 202310611117).

Declarations

Conflict of interest The authors declare that there is no conflict of interest.

References

1. Krevor S, de Coninck H, Gasda SE et al (2023) Subsurface carbon dioxide and hydrogen storage for a sustainable energy future. Nat Rev Earth Environ 4:102–118
2. Liu R, Wang ZL, Fukuda K et al (2022) Flexible self-charging power sources. Nat Rev Mater 7:870–886
3. Quilty CD, Wu D, Li W et al (2023) Electron and ion transport in lithium and lithium-ion battery negative and positive composite electrodes. Chem Rev 123(4):1327–1363
4. Fang S, Zhang J, Niu Y et al (2023) Removal of nitrate nitrogen from wastewater by green synthetic hydrophilic activated carbon supported sulfide modified nanoscale zerovalent iron: characterization, performance and mechanism. Chem Eng J 461:141990
5. Abouhaswa AS, Selezneva NV, Merentsov AI et al (2017) Phase relations and structure–properties correlations in Fe (S, Se, Te). Phys C Supercond Appl 539:19–24
6. Harman WH (2023) Stabilizing sulfur: synthesis of a terminal FeIII=S complex. Chem 9(9):2368–2370
7. Kim YB, Seo HY, Kim KH et al (2024) Synthesis of iron sulfide nanocrystals encapsulated in highly porous carbon-coated CNT microsphere as anode materials for sodium-ion batteries. Small 20(7):e2305686
8. Zhang H, Geng Y, Huang J et al (2023) Charge and mass transport mechanisms in two-dimensional covalent organic frameworks (2D COFs) for electrochemical energy storage devices. Energy Environ Sci 16(3):889–951
9. Wei H, Dai J, Maharik I et al (2022) Simultaneous synthesis of H_2, O_2, and N_2 via an innovatory energy system in Coronavirus pandemic time: design, techno-economic assessment, and optimization approaches. Int J Hydrogen Energy 47(62):26038–26052
10. Liu Z, Wang J, Bi R et al (2023) Ultrasmall NiS_2 nanocrystals embedded in ordered macroporous graphenic carbon matrix for efficiently pseudocapacitive sodium storage. Trans Tianjin Univ 29(2):89–100
11. Gan Z, Yin J, Xu X et al (2022) Nanostructure and advanced energy storage: elaborate material designs lead to high-rate pseudocapacitive ion storage. ACS Nano 16(4):5131–5152
12. Kandpal S, Ghosh T, Rani C et al (2023) Multifunctional electrochromic devices for energy applications. ACS Energy Lett 8(4):1870–1886
13. Zhu Z, Jiang T, Ali M et al (2022) Rechargeable batteries for grid scale energy storage. Chem Rev 122(22):16610–16751
14. Yu S, Hong Ng VM, Wang F et al (2018) Synthesis and application of iron-based nanomaterials as anodes of lithium-ion batteries and supercapacitors. J Mater Chem A 6(20):9332–9367
15. Cao Z, Song H, Cao B et al (2017) Sheet-on-sheet chrysanthemum-like C/FeS microspheres synthesized by one-step solvothermal method for high-performance sodium-ion batteries. J Power Sources 364:208–214
16. Fang L, Ma R, Gao XJ et al (2022) Metastable iron sulfides gram-dependently counteract resistant Gardnerella vaginalis for bacterial vaginosis treatment. Adv Sci 9(10):e2104341
17. Jin X, Shan Y, Sun F et al (2022) Applications of transition metal (Fe, co, Ni)-based metal–organic frameworks and their derivatives in batteries and supercapacitors. Trans Tianjin Univ 28(6):446–468
18. Durga IK, Rao SS, Kalla RMN et al (2020) Facile synthesis of FeS_2/PVP composite as high-performance electrodes for supercapacitors. J Energy Storage 28:101216
19. Chen X, Zhang L, Cui J et al (2024) Semiconductor-to-metal transition renders intrinsic pseudocapacitance and high volumetric capacity for iron chalcogenide anode. Chem Eng J 480:147979
20. Liu Y, Zuo Z, Li H et al (2023) In-situ advanced oxidation of sediment iron for sulfide control in sewers. Water Res 240:120077
21. Mei J, Deng Y, Cheng X et al (2024) Recent advances in iron-based sulfides electrocatalysts for oxygen and hydrogen evolution reaction. Chin Chem Lett 35(1):108900
22. Shao B, Tan S, Huang Y et al (2022) Enabling conversion-type iron fluoride cathode by halide-based solid electrolyte. Adv Funct Mater 32(49):2206845
23. Sherbow TJ, Fu W, Tao L et al (2022) Thionitrite (SNO-) and perthionitrite (SSNO-) are simple synthons for nitrosylated iron sulfur clusters. Angew Chem Int Ed Engl 61(30):e202204570
24. Tarek M, Santos JS, Márquez V et al (2024) A critical review towards the causes of the iron-based catalysts deactivation mechanisms in the selective oxidation of hydrogen sulfide to elemental sulfur from biogas. J Energy Chem 90:388–411
25. Zhang P, Zhu Q, Soomro RA et al (2020) In situ ice template approach to fabricate 3D flexible MXene film-based electrode for high performance supercapacitors. Adv Funct Mater 30(47):2000922
26. Valdez-Moreira JA, Wannipurage DC, Pink M et al (2023) Hydrogen atom abstraction by a high spin [FeIII=S] complex. Chem 9(9):2601–2609

27. Villanueva N, Alegre C, Rubin J et al (2022) Iron electrodes based on sulfur-modified iron oxides with enhanced stability for iron–air batteries. ACS Appl Energy Mater 5(11):13439–13451
28. Xie Q, Lan M, Li B et al (2022) Interface engineering of iron sulfide/tungsten nitride heterostructure catalyst for boosting oxygen reduction activity. Chem Eng J 431:133274
29. Yu J, Yang S, Liu D et al (2023) Interaction of chromium-sulfur-iron during Cr(VI) stabilization by polysulfide-modified nanoscale zero-valent iron for groundwater remediation: batch experiments and numerical simulation. Chem Eng J 475:146233
30. Zhao F, Xiao J, Geng S et al (2022) Novel Fe_7S_8/C nanocomposites with accelerating iron cycle for enhanced heterogeneous electro-Fenton degradation of dyes. Electrochim Acta 436:141381
31. Song Z, Wang Z, Yu R (2024) Strategies for advanced supercapacitors based on 2D transition metal dichalcogenides: from material design to device setup. Small Methods 8(1):e2300808
32. Rui X, Tan H, Yan Q (2014) Nanostructured metal sulfides for energy storage. Nanoscale 6(17):9889–9924
33. Ji Z, Chen L, Tang G et al (2024) Rational design of high-performance electrodes based on ferric oxide nanosheets deposited on reduced graphene oxide for advanced hybrid supercapacitors. Small 20(15):e2306236
34. Ma J, Guo X, Yan Y et al (2018) FeO_x-based materials for electrochemical energy storage. Adv Sci 5(6):1700986
35. Zhang D, Han X, Kong X et al (2020) The principle of introducing halogen ions into β-FeOOH: controlling electronic structure and electrochemical performance. Nanomicro Lett 12(1):107
36. Jia Y, Ma Y (2024) Advances in MoO_3-based supercapacitors for electrochemical energy storage. J Energy Storage 85:111103
37. Gujar TP, Shinde VR, Lokhande CD et al (2006) Electrosynthesis of Bi_2O_3 thin films and their use in electrochemical supercapacitors. J Power Sources 161(2):1479–1485
38. Guan J, Chen Y, Cao L et al (2020) Multicomponent design of Fe_3O_4 nanosheet-based binder-free anodes with a special substrate for supercapacitors. J Power Sources 469:228307
39. Uma Shankar V, Govindarajan D, Gopalakrishnan R et al (2021) rGO-encapsulated Sn-doped V_2O_5 nanorods for high-performance supercapacitors. Mater Today Commun 27:102357
40. Gamby J, Taberna PL, Simon P et al (2001) Studies and characterisations of various activated carbons used for carbon/carbon supercapacitors. J Power Sources 101(1):109–116
41. Teo EYL, Muniandy L, Ng EP et al (2016) High surface area activated carbon from rice husk as a high performance supercapacitor electrode. Electrochim Acta 192:110–119
42. An KH, Kim WS, Park YS et al (2001) Supercapacitors using single-walled carbon nanotube electrodes. Adv Mater 13(7):497–500
43. An KH, Kim WS, Park YS et al (2001) Electrochemical properties of high-power supercapacitors using single-walled carbon nanotube electrodes. Adv Funct Mater 11(5):387–392
44. Fan Z, Yan J, Zhi L et al (2010) A three-dimensional carbon nanotube/graphene sandwich and its application as electrode in supercapacitors. Adv Mater 22(33):3723–3728
45. Yoo JJ, Balakrishnan K, Huang J et al (2011) Ultrathin planar graphene supercapacitors. Nano Lett 11(4):1423–1427
46. Qu D (2002) Studies of the activated carbons used in double-layer supercapacitors. J Power Sources 109(2):403–411
47. Alaş MÖ, Güngör A, Genç R et al (2019) Feeling the power: robust supercapacitors from nanostructured conductive polymers fostered with Mn^{2+} and carbon dots. Nanoscale 11(27):12804–12816
48. Li K, Wang X, Wang X et al (2020) All-pseudocapacitive asymmetric MXene-carbon-conducting polymer supercapacitors. Nano Energy 75:104971
49. Wei J, Li X, Xue H et al (2018) Hollow structural transition metal oxide for advanced supercapacitors. Adv Mater Interfaces 5(9):1701509
50. Moosavifard SE, El-Kady MF, Rahmanifar MS et al (2015) Designing 3D highly ordered nanoporous CuO electrodes for high-performance asymmetric supercapacitors. ACS Appl Mater Interfaces 7(8):4851–4860
51. Chen J, Chen H, Chen M et al (2022) Nacre-inspired surface-engineered MXene/nanocellulose composite film for high-performance supercapacitors and zinc-ion capacitors. Chem Eng J 428:131380
52. Li J, Wang H, Xiao X (2020) Intercalation in two-dimensional transition metal carbides and nitrides (MXenes) toward electrochemical capacitor and beyond. Energy & Environ Mater 3(3):306–322
53. Choudhary N, Li C, Chung HS et al (2016) High-performance one-body core/shell nanowire supercapacitor enabled by conformal growth of capacitive 2D WS_2 layers. ACS Nano 10(12):10726–10735
54. Luo W, Zhang G, Cui Y et al (2017) One-step extended strategy for the ionic liquid-assisted synthesis of Ni_3S_4–MoS_2 heterojunction electrodes for supercapacitors. J Mater Chem A 5(22):11278–11285
55. Chen F, Liu C, Cui B et al (2021) Regulated synthesis of Eutectic Ni_3S_2/NiS nanorods for quasi-solid-state hybrid supercapacitors with high energy density. J Power Sources 482:228910
56. Singhal R, Chaudhary M, Tyagi S et al (2022) Recent developments in transition metal-based nanomaterials for supercapacitor applications. J Mater Res 37(13):2124–2149
57. Veerakumar P, Sangili A, Manavalan S et al (2020) Research progress on porous carbon supported metal/metal oxide nanomaterials for supercapacitor electrode applications. Ind Eng Chem Res 59(14):6347–6374
58. Owusu KA, Qu L, Li J et al (2017) Low-crystalline iron oxide hydroxide nanoparticle anode for high-performance supercapacitors. Nat Commun 8:14264
59. Zheng L, Song J, Ye X et al (2020) Construction of self-supported hierarchical NiCo-S nanosheet arrays for supercapacitors with ultrahigh specific capacitance. Nanoscale 12(25):13811–13821
60. Qu Q, Yang S, Feng X (2011) 2D sandwich-like sheets of iron oxide grown on graphene as high energy anode material for supercapacitors. Adv Mater 23(46):5574–5580
61. Chen YC, Lin YG, Hsu YK et al (2014) Novel iron oxyhydroxide lepidocrocite nanosheet as ultrahigh power density anode material for asymmetric supercapacitors. Small 10(18):3803–3810
62. Lee JS, Shin DH, Jun J et al (2014) Fe_3O_4/carbon hybrid nanoparticle electrodes for high-capacity electrochemical capacitors. Chemsuschem 7(6):1676–1683
63. Chen G, Ma C, Fu Z et al (2022) Significantly enhancing fracture toughness of epoxy composite with promising γ-FeOOH@Fe_2O_3 hybrid nanoparticles by magnetic field assistance. Nano Mater Sci 4(2):139–150
64. Yang T, Niu Y, Liu Q et al (2023) Cathode host engineering for non-lithium (Na, K and Mg) sulfur/selenium batteries: a state-of-the-art review. Nano Mater Sci 5(2):119–140
65. Yamaguchi Y, Takeuchi T, Sakaebe H et al (2010) Ab initio simulations of Li/pyrite-MS_2 (M=Fe, Ni) battery cells. J Electrochem Soc 157(6):A630
66. Kim BC, Takada K, Ohta N et al (2005) All solid state Li-ion secondary battery with FeS anode. Solid State Ion 176(31–34):2383–2387
67. Pham DT, Baboo JP, Song J et al (2018) Facile synthesis of pyrite (FeS_2/C) nanoparticles as an electrode material for non-aqueous hybrid electrochemical capacitors. Nanoscale 10(13):5938–5949

68. Rajeswari J, Kishore PS, Viswanathan B et al (2009) One-dimensional MoO_2 nanorods for supercapacitor applications. Electrochem Commun 11(3):572–575
69. Xu H, Hu X, Yang H et al (2015) Flexible asymmetric microsupercapacitors based on Bi_2O_3 and MnO_2 nanoflowers: larger areal mass promises higher energy density. Adv Energy Mater 5(6):1401882
70. Chaudhari NK, Chaudhari S, Yu JS (2014) Cube-like α-Fe_2O_3 supported on ordered multimodal porous carbon as high performance electrode material for supercapacitors. Chemsuschem 7(11):3102–3111
71. Guan D, Gao Z, Yang W et al (2013) Hydrothermal synthesis of carbon nanotube/cubic Fe_3O_4 nanocomposite for enhanced performance supercapacitor electrode material. Mater Sci Eng B 178(10):736–743
72. Chang J, Jin M, Yao F et al (2013) Asymmetric supercapacitors based on graphene/MnO_2 nanospheres and graphene/MoO_3 nanosheets with high energy density. Adv Funct Mater 23(40):5074–5083
73. Chen Z, Augustyn V, Wen J et al (2011) High-performance supercapacitors based on intertwined CNT/V_2O_5 nanowire nanocomposites. Adv Mater 23(6):791–795
74. Gao Z, Yang W, Wang J et al (2015) Flexible all-solid-state hierarchical $NiCo_2O_4$/porous graphene paper asymmetric supercapacitors with an exceptional combination of electrochemical properties. Nano Energy 13:306–317
75. Zeng Y, Han Y, Zhao Y et al (2015) Advanced Ti-doped Fe_2O_3@PEDOT core/shell anode for high-energy asymmetric supercapacitors. Adv Energy Mater 5(12):1402176
76. Lu X, Zeng Y, Yu M et al (2014) Oxygen-deficient hematite nanorods as high-performance and novel negative electrodes for flexible asymmetric supercapacitors. Adv Mater 26(19):3148–3155
77. Yang P, Ding Y, Lin Z et al (2014) Low-cost high-performance solid-state asymmetric supercapacitors based on MnO_2 nanowires and Fe_2O_3 nanotubes. Nano Lett 14(2):731–736
78. Liu D, Xu L, Xie J et al (2019) A perspective of chalcogenide semiconductor-noble metal nanocomposites through structural transformations. Nano Mater Sci 1(3):184–197
79. Yuan S, Fan W, Jin Y et al (2021) Free-standing flexible graphene-based aerogel film with high energy density as an electrode for supercapacitors. Nano Mater Sci 3(1):68–74
80. Wang X, Xiao Z, Zhao Z et al (2023) Construction of iron/cobalt disulfides nanoparticles anchored on biomass-derived hierarchically porous carbon for hybrid supercapacitors with ultrahigh energy density. J Alloys Compd 935:168074
81. Turali-Emre ES, Emre AE, Vecchio DA et al (2023) Self-organization of iron sulfide nanoparticles into complex multicompartment supraparticles. Adv Mater 35(23):e2211244
82. Heift D, Lacroix LM, Lecante P et al (2018) Controlling the sulfidation process of iron nanoparticles: accessing iron–iron sulfide core-shell structures. ChemNanoMat 4(7):663–669
83. Talande SV, Bakandritsos A, Zdražil L et al (2020) Pinning ultrasmall greigite nanoparticles on graphene for effective transition-metal-sulfide supercapacitors in an ionic liquid electrolyte. J Mater Chem A 8(48):25716–25726
84. Azimov F, Lee J, Park S et al (2023) Fabrication of assembled FeS_2 nanosheet and application for high-performance supercapacitor electrodes. ACS Appl Mater Interfaces 15(22):26967–26976
85. Cai J, Lai CL, Sun PX et al (2022) 3 electrons donator-FeS/C composite anode for supercapacitor. J Mater Sci Mater Electron 33(36):26966–26979
86. Zhang F, Wang C, Huang G et al (2016) FeS_2@C nanowires derived from organic-inorganic hybrid nanowires for high-rate and long-life lithium-ion batteries. J Power Sources 328:56–64
87. Huang Y, Zhao Y, Bao J et al (2019) Lawn-like $FeCo_2S_4$ hollow nanoneedle arrays on flexible carbon nanofiber film as binder-free electrodes for high-performance asymmetric pseudocapacitors. J Alloys Compd 772:337–347
88. Wang Z, Liu C, Shi G et al (2020) Preparation and electrochemical properties of electrospun FeS/carbon nanofiber composites. Ionics 26(6):3051–3060
89. Kuo TR, Chen WT, Liao HJ et al (2017) Improving hydrogen evolution activity of earth-abundant cobalt-doped iron pyrite catalysts by surface modification with phosphide. Small. https://doi.org/10.1002/smll.201603356
90. Pan K, Zhai Y, Zhang J et al (2019) FeS_2/C nanowires as an effective catalyst for oxygen evolution reaction by electrolytic water splitting. Materials 12(20):3364
91. Fang Y, Luan D, Gao S et al (2021) Rational design and engineering of one-dimensional hollow nanostructures for efficient electrochemical energy storage. Angew Chem Int Ed Engl 60(37):20102–20118
92. Premkumar M, Vadivel S (2023) Fabrication of binder-free CNT/$FeNiS_2$@PPy mixed metal sulfide loaded Ni foam as cathode material for asymmetric supercapacitor applications. J Energy Storage 69:107948
93. Ma T, Liu H, Wang Y et al (2019) Rapid construction of three-dimensional sulfur doped graphene supported by $NiFeS_2$ interconnected networks as convenient electron/ion transport channels for flexible supercapacitors. Electrochim Acta 309:1–10
94. Velmurugan R, Amuthan D, Saranyan V et al (2023) In situ moulded troilite 2H phase FeS ultrathin electrodes via pulsed laser deposition for flexible solid state high capacity supercapacitor besides boosted electrocatalytic oxygen evolution reaction. J Mater Chem A 11(10):5148–5165
95. Liang Q, Zhong L, Du C et al (2018) Achieving highly efficient electrocatalytic oxygen evolution with ultrathin 2D Fe-doped nickel thiophosphate nanosheets. Nano Energy 47:257–265
96. Luan X, Du H, Kong Y et al (2019) A novel FeS-NiS hybrid nanoarray: an efficient and durable electrocatalyst for alkaline water oxidation. Chem Commun 55(51):7335–7338
97. Wang C, Li K, Sun Q et al (2023) Diatomite-like $KFeS_2$ for use in high-performance electrodes for energy storage and oxygen evolution. Nanomaterials 13(4):643
98. Wu ZS, Sun Y, Tan YZ et al (2012) Three-dimensional graphene-based macro- and mesoporous frameworks for high-performance electrochemical capacitive energy storage. J Am Chem Soc 134(48):19532–19535
99. Yu Y, Addai-Mensah J, Losic D (2010) Synthesis of self-supporting gold microstructures with three-dimensional morphologies by direct replication of diatom templates. Langmuir 26(17):14068–14072
100. Zhang YX, Huang M, Li F et al (2014) One-pot synthesis of hierarchical MnO_2-modified diatomites forelectrochemical capacitor electrodes. J Power Sources 246:449–456
101. Dai X, Rao J, Bao Z et al (2022) Magnetic double-core@shell MnO_2@NiFe@DE as a multifunctional scavenger for efficient removal of tetracycline, anionic and cationic dyes. J Colloid Interface Sci 628(Pt A):769–783
102. Li K, Teng H, Sun Q et al (2022) Engineering active sites on nitrogen-doped carbon nanotubes/cobaltosic oxide heterostructure embedded in biotemplate for high-performance supercapacitors. J Energy Storage 53:105094
103. Pei L, Yang Y, Chu H et al (2016) Self-assembled flower-like FeS_2/graphene aerogel composite with enhanced electrochemical properties. Ceram Int 42(4):5053–5061
104. Stankovich S, Dikin DA, Piner RD et al (2007) Synthesis of graphene-based nanosheets via chemical reduction of exfoliated graphite oxide. Carbon 45(7):1558–1565

105. Xiao L, Wu D, Han S et al (2013) Self-assembled Fe_2O_3/graphene aerogel with high lithium storage performance. ACS Appl Mater Interfaces 5(9):3764–3769
106. Mohammadi Zardkhoshoui A, Hosseiny Davarani SS, Maleka Ashtiani M et al (2019) Designing an asymmetric device based on graphene wrapped yolk–double shell $NiGa_2S_4$ hollow microspheres and graphene wrapped FeS_2–$FeSe_2$ core–shell cratered spheres with outstanding energy density. J Mater Chem A 7(17):10282–10292
107. Fan M, Zhang L, Li K et al (2019) FeS_2@C core–shell nanochains as efficient electrocatalysts for hydrogen evolution reaction. ACS Appl Nano Mater 2(6):3889–3896
108. Guo M, Qayum A, Dong S et al (2020) In situ conversion of metal (Ni, Co or Fe) foams into metal sulfide (Ni_3S_2, Co_9S_8 or FeS) foams with surface grown N-doped carbon nanotube arrays as efficient superaerophobic electrocatalysts for overall water splitting. J Mater Chem A 8(18):9239–9247
109. Zhong Y, Liu J, Lu Z et al (2016) Hierarchical FeS_2 nanosheet@Fe_2O_3 nanosphere heterostructure as promising electrode material for supercapacitors. Mater Lett 166:223–226
110. Shao X, Zhu Z, Zhao C et al (2018) Hierarchical FeS/RGO/FeS@Fe foil as high-performance negative electrode for asymmetric supercapacitors. Inorg Chem Front 5(8):1912–1922
111. Zhao C, Shao X, Zhu Z et al (2017) One-pot hydrothermal synthesis of RGO/FeS composite on Fe foil for high performance supercapacitors. Electrochim Acta 246:497–506
112. Javed MS, Najam T, Sajjad M et al (2021) Design and fabrication of highly porous 2D bimetallic sulfide ZnS/FeS composite nanosheets as an advanced negative electrode material for supercapacitors. Energy Fuels 35(18):15185–15191
113. Huang Y, Zhao H, Bao S et al (2022) Hollow FeS_2 nanospheres encapsulated in N/S Co-doped carbon nanofibers as electrode material for electrochemical energy storage. J Alloys Compd 905:164184
114. Pant B, Pant HR, Park M (2020) $Fe_{1-x}S$ modified TiO_2 NPs embedded carbon nanofiber composite via electrospinning: a potential electrode material for supercapacitors. Molecules 25(5):1075
115. Zhang Y, Xu M, Wang Y et al (2020) Spray drying-assisted preparation FeS_x/C/CNT composite for energy storage and conversion performance. J Alloys Compd 834:154916
116. Sun Z, Lin H, Zhang F et al (2018) Rapid microwave-assisted synthesis of high-rate FeS_2 nanoparticles anchored on graphene for hybrid supercapacitors with ultrahigh energy density. J Mater Chem A 6(30):14956–14966
117. Yan SX, Luo SH, Liu H et al (2022) In-situ partial reduction-sulfurized Fe_3O_4@FeS based on pickling iron red as a versatile electrode for high-performance lithium ion batteries and supercapacitor devices. Surf Coat Technol 429:127980
118. Karade SS, Dwivedi P, Majumder S et al (2017) First report on a FeS-based 2 V operating flexible solid-state symmetric supercapacitor device. Sustain Energy Fuels 1(6):1366–1375
119. Sonia YK, Meher SK (2022) Electrostructural compatibility of battery-type diffuse-porous Co_9S_8–$NiCo_2S_4$/defective reduced graphene oxide and flaky FeS/nitrogen-doped defective reduced graphene oxide for ultra-high-performance all-solid-state hybrid pseudocapacitors. ACS Appl Energy Mater 5(11):13672–13691
120. Ikkurthi KD, Srinivasa Rao S, Jagadeesh M et al (2018) Synthesis of nanostructured metal sulfides via a hydrothermal method and their use as an electrode material for supercapacitors. New J Chem 42(23):19183–19192
121. Dong X, Jin H, Wang R et al (2018) High volumetric capacitance, ultralong life supercapacitors enabled by waxberry-derived hierarchical porous carbon materials. Adv Energy Mater 8(11):1702695
122. Zhu J, Tang S, Wu J et al (2017) Wearable high-performance supercapacitors based on silver-sputtered textiles with $FeCo_2S_4$–$NiCo_2S_4$ composite nanotube-built multitripod architectures as advanced flexible electrodes. Adv Energy Mater 7(2):1601234
123. Upadhyay KK, Bundaleska N, Abrashev M et al (2022) Free-standing graphene-carbon as negative and FeCoS as positive electrode for asymmetric supercapacitor. J Energy Storage 50:104637
124. Li K, Hu Z, Zhao R et al (2021) A multidimensional rational design of nickel-iron sulfide and carbon nanotubes on diatomite via synergistic modulation strategy for supercapacitors. J Colloid Interface Sci 603:799–809
125. Béguin F, Presser V, Balducci A et al (2014) Carbons and electrolytes for advanced supercapacitors. Adv Mater 26(14):2219–2251
126. Jiang Y, Liu J (2019) Definitions of pseudocapacitive materials: a brief review. Energy & Environ Mater 2(1):30–37
127. Qiu Z, Wang Y, Bi X et al (2018) Biochar-based carbons with hierarchical micro-meso-macro porosity for high rate and long cycle life supercapacitors. J Power Sources 376:82–90
128. Miao L, Song Z, Zhu D et al (2020) Recent advances in carbon-based supercapacitors. Mater Adv 1(5):945–966
129. Kumar S, Saeed G, Zhu L et al (2021) 0D to 3D carbon-based networks combined with pseudocapacitive electrode material for high energy density supercapacitor: a review. Chem Eng J 403:126352
130. Ren K, Liu Z, Wei T et al (2021) Recent developments of transition metal compounds-carbon hybrid electrodes for high energy/power supercapacitors. Nanomicro Lett 13(1):129
131. Xu X, Cai T, Meng Z et al (2016) FeS_2 nanocrystals prepared in hierarchical porous carbon for lithium-ion battery. J Power Sources 331:366–372
132. Brownson DAC, Kampouris DK, Banks CE (2011) An overview of graphene in energy production and storage applications. J Power Sources 196(11):4873–4885
133. Sankar KV, Kalai Selvan R (2015) Improved electrochemical performances of reduced graphene oxide based supercapacitor using redox additive electrolyte. Carbon 90:260–273
134. Zhou X, Yin YX, Cao AM et al (2012) Efficient 3D conducting networks built by graphene sheets and carbon nanoparticles for high-performance silicon anode. ACS Appl Mater Interfaces 4(5):2824–2828
135. Zhao C, Shao X, Zhang Y et al (2016) Fe_2O_3/reduced graphene oxide/Fe_3O_4 composite in situ grown on Fe foil for high-performance supercapacitors. ACS Appl Mater Interfaces 8(44):30133–30142
136. Wang X, Wei Q, Li H et al (2022) Iron-chalcogenide-based electrode materials for electrochemical energy storage. J Mater Chem A 10(14):7517–7556
137. Von Lim Y, Li XL, Yang HY (2021) Recent tactics and advances in the application of metal sulfides as high-performance anode materials for rechargeable sodium-ion batteries. Adv Funct Mater 31(10):2006761
138. Tao Y, Yuan J, Qian X et al (2021) Spinel-type $FeNi_2S_4$ with rich sulfur vacancies grown on reduced graphene oxide toward enhanced supercapacitive performance. Inorg Chem Front 8(9):2271–2279
139. Meng Q, Cai K, Chen Y et al (2017) Research progress on conducting polymer based supercapacitor electrode materials. Nano Energy 36:268–285
140. Shi Y, Peng L, Ding Y et al (2015) Nanostructured conductive polymers for advanced energy storage. Chem Soc Rev 44(19):6684–6696
141. Zeng R, Li Z, Li L et al (2019) Covalent connection of polyaniline with MoS_2 nanosheets toward ultrahigh rate capability supercapacitors. ACS Sustain Chem Eng 7(13):11540–11549

142. Zhu J, Sun W, Yang D et al (2015) Multifunctional architectures constructing of PANI nanoneedle arrays on MoS_2 thin nanosheets for high-energy supercapacitors. Small 11(33):4123–4129
143. Samtham M, Singh D, Hareesh K et al (2022) Perspectives of conducting polymer nanostructures for high-performance electrochemical capacitors. J Energy Storage 51:104418
144. Son SB, Yersak TA, Piper DM et al (2014) A stabilized PAN-FeS_2 cathode with an EC/DEC liquid electrolyte. Adv Energy Mater 4(3):1300961
145. Tan C, Zhang H (2015) Two-dimensional transition metal dichalcogenide nanosheet-based composites. Chem Soc Rev 44(9):2713–2731
146. Wang H, Dai H (2013) Strongly coupled inorganic–nanocarbon hybrid materials for energy storage. Chem Soc Rev 42(7):3088–3113
147. Aslan M, Weingarth D, Jäckel N et al (2014) Polyvinylpyrrolidone as binder for castable supercapacitor electrodes with high electrochemical performance in organic electrolytes. J Power Sources 266:374–383
148. Hsin YL, Hwang KC, Yeh CT (2007) Poly(vinylpyrrolidone)-modified graphite carbon nanofibers as promising supports for PtRu catalysts in direct methanol fuel cells. J Am Chem Soc 129(32):9999–10010
149. Cai M, Qian H, Wei Z et al (2014) Polyvinyl pyrrolidone-assisted synthesis of a Fe_3O_4/graphene composite with excellent lithium storage properties. RSC Adv 4(13):6379–6382
150. Zhang X, Wang J, Jia H et al (2016) Polyvinyl pyrrolidone modified graphene oxide for improving the mechanical, thermal conductivity and solvent resistance properties of natural rubber. RSC Adv 6(60):54668–54678
151. Joshi KV, Joshi BK, Harikrishnan U et al (2013) Polyvinyl pyrrolidone modified ZnS nanoparticles as a highly selective and sensitive nanosensor for the iodide ion. Anal Methods 5(19):4973–4977
152. Saini S, Shah J, Kotnala RK et al (2020) Nickel substituted oxygen deficient nanoporous lithium ferrite based green energy device hydroelectric cell. J Alloys Compd 827:154334
153. Shaddad MN, Arunachalam P, Hezam M et al (2021) Unprecedented solar water splitting of dendritic nanostructured Bi_2O_3 films by combined oxygen vacancy formation and Na_2MoO_4 doping. Int J Hydrog Energy 46(46):23702–23714
154. Voigt B, Das B, Carr DM et al (2021) Mitigation of the internal p-n junction in CoS_2-contacted FeS_2 single crystals: accessing bulk semiconducting transport. Phys Rev Materials 5(2):025405
155. Lin J, Wang Y, Zheng X et al (2018) P-doped $NiCo_2S_4$ nanotubes as battery-type electrodes for high-performance asymmetric supercapacitors. Dalton Trans 47(26):8771–8778
156. Meng Y, Sun P, He W et al (2019) Uniform P doped Co–Ni–S nanostructures for asymmetric supercapacitors with ultra-high energy densities. Nanoscale 11(2):688–697
157. Jiang B, Ban X, Wang Q et al (2019) Anionic P-substitution toward ternary Ni–S–P nanoparticles immobilized graphene with ultrahigh rate and long cycle life for hybrid supercapacitors. J Mater Chem A 7(42):24374–24388
158. Venkateshalu S, Goban Kumar P, Kollu P et al (2018) Solvothermal synthesis and electrochemical properties of phase pure pyrite FeS_2 for supercapacitor applications. Electrochim Acta 290:378–389
159. Sun Z, Li F, Ma Z et al (2021) Battery-type phosphorus doped FeS_2 grown on graphene as anode for hybrid supercapacitor with enhanced specific capacity. J Alloys Compd 854:157114
160. Ahmed A, Naseem Siddique M, Alam U et al (2019) Improved photocatalytic activity of Sr doped SnO_2 nanoparticles: a role of oxygen vacancy. Appl Surf Sci 463:976–985
161. Al-Namshah KS, Shkir M, Hamdy MS (2021) Enhanced photocatalytic performance of one-pot flash combustion synthesized ZnO nanoparticles: an effect of Bi doping. J Inorg Organomet Polym Mater 31(11):4338–4348
162. Gakhar T, Hazra A (2020) Oxygen vacancy modulation of titania nanotubes by cathodic polarization and chemical reduction routes for efficient detection of volatile organic compounds. Nanoscale 12(16):9082–9093
163. Han Z, Choi C, Hong S et al (2019) Activated TiO_2 with tuned vacancy for efficient electrochemical nitrogen reduction. Appl Catal B Environ 257:117896
164. Yan Z, Sun Z, Zhao L et al (2022) In-situ induced sulfur vacancy from phosphorus doping in FeS_2 microflowers for high-efficiency lithium storage. Mater Today Nano 20:100261
165. Yan Z, Sun Z, Guo Z et al (2022) Quantitatively tunable anionic vacancies of iron disulfide nanorods with superior cyclability and rate capability for Li-ion batteries. ACS Appl Energy Mater 5(7):8563–8572
166. Pan Y, Yu E, Wang D et al (2021) Sulfur vacancy enhances the electronic and optical properties of FeS_2 as the high performance electrode material. J Alloys Compd 858:157662
167. Shao Z, Meng H, Sun J et al (2020) Engineering of amorphous structures and sulfur defects into ultrathin FeS nanosheets to achieve superior electrocatalytic alkaline oxygen evolution. ACS Appl Mater Interfaces 12(46):51846–51853
168. Li D, Zhao L, Xia Q et al (2022) Activating MoS_2 nanoflakes via sulfur defect engineering wrapped on CNTs for stable and efficient Li-O_2 batteries. Adv Funct Mater 32(8):2108153
169. Wang J, Fang J, Zhao H et al (2021) Raspberry-like hierarchical structure FeS_2 decorated by dual-carbon framework as high-performance cathode for rechargeable lithium batteries. Carbon 171:171–178
170. Wang J, Huang J, Huang S et al (2020) Rational design of hierarchical SnS_2 microspheres with S vacancy for enhanced sodium storage performance. ACS Sustain Chem Eng 8(25):9519–9525
171. Wang J, Zhao Y, Li G et al (2021) Aligned sulfur-deficient ZnS_{1-x} nanotube arrays as efficient catalyzer for high-performance lithium/sulfur batteries. Nano Energy 84:105891
172. Zhao Y, Yang D, He T et al (2021) Vacancy engineering in VS_2 nanosheets for ultrafast pseudocapacitive sodium ion storage. Chem Eng J 421:129715

Can Wang is currently an undergraduate student in Prof. Yuxin Zhang's group, Chongqing University. His research interest focusses on the preparation and application of nanomaterials for electrodes and electrocatalyst.

Yuxin Zhang received his B.Eng. and M.Eng degrees in chemical engineering from Tianjin University, China, in 2000 and 2003, respectively. He received his Ph.D. degree in chemistry and biomolecular engineering from the National University of Singapore (NUS), Singapore, in 2008, and continued to work as a research fellow in Prof. Huachun ZENG's group at NUS until 2009. His research interests involve the preparation and application of nanomaterials, synthesis and morphology control of electrode materials in supercapacitors, and advanced design and performance research of photocatalytic materials.

Shude Liu is currently a professor at the College of Textiles, Donghua University (China), and a visiting professor at Nagoya University (Japan). He obtained his PhD from the School of Mechanical Engineering, Yonsei University, South Korea, in 2020. From 2021 to 2023, he was a JSPS fellow and postdoctoral researcher in the ERATO program at the National Institute for Materials Science, Japan. His research interests include the design and preparation of flexible electrode materials, surface and interface chemistry of materials, electrode failure analysis, and the development and application of self-powered smart textiles.